





Article

New Insights into the Materials and Painting Techniques of Ancient Wall Paintings from the Roman Province of Dacia: A Minimally Invasive Multi-Method Approach

Ioana Maria Cortea ^{1,*} , Luminița Ghervase ¹ , Lucian Ratoiu ¹ , Ovidiu Țentea ² and Monica Dinu ¹ 

¹ Department of Optoelectronic Methods and Techniques for Artwork Restoration and Conservation, National Institute of Research and Development for Optoelectronics—INOE 2000, 077125 Magurele, Romania; ghervase@inoe.ro (L.G.); lucian@inoe.ro (L.R.); monica.dinu@inoe.ro (M.D.)

² Department of Archaeology, National Museum of Romanian History, 030024 Bucharest, Romania; ovidiu@mnir.ro

* Correspondence: ioana.cortea@inoe.ro

Abstract: A group of wall painting fragments discovered at Ulpia Traiana Sarmizegetusa, an important Roman archeological site located in the former Roman province of Dacia (Romania), have been investigated with the aim of defining the material composition of their pictorial layers and exploring the pictorial technology used. In order to preserve the integrity of the murals and minimize sampling, an array of non- and micro-invasive techniques has been employed, including X-ray fluorescence, laser-induced breakdown spectroscopy, Fourier transform infrared spectroscopy, and hyperspectral imaging. In accordance with previous studies, the identified color palette was mainly based on iron-rich earth pigments (red and yellow ochres, green earth) and carbon-based blacks (soot/charcoal, bone black). Egyptian blue, lazurite, some lead-based pigments, and potentially indigo were also identified (in complex mixtures) on the uppermost paint layers, typically applied *a secco* over the *a fresco* background. The presence of expensive pigments and the existence of a red preparatory drawing, documented for the first time in the region, indicate that the original wall paintings had elaborate schemes and, secondly, reflect the patron's wealth and social status. Hyperspectral imaging was able to retrieve some faded paint layers in certain cases, helping to recover lost decorative details, an indicator of a more complex polychromy compared to what we see today. The obtained results add important contributions to the limited corpus of data regarding the technical know-how of decorative polychrome painting on plaster found in Roman archeological sites in Romania.

Keywords: Roman wall paintings; pigments; organic binders; spectroscopy; XRF; LIBS; FTIR; hyperspectral imaging; archeological findings; cultural heritage



Citation: Cortea, I.M.; Ghervase, L.; Ratoiu, L.; Țentea, O.; Dinu, M. New Insights into the Materials and Painting Techniques of Ancient Wall Paintings from the Roman Province of Dacia: A Minimally Invasive Multi-Method Approach. *Heritage* **2024**, *7*, 5268–5294. <https://doi.org/10.3390/heritage7090248>

Academic Editor: Nicola Masini

Received: 22 August 2024

Revised: 12 September 2024

Accepted: 18 September 2024

Published: 21 September 2024



Copyright: © 2024 by the authors. Licensee MDPI, Basel, Switzerland. This article is an open access article distributed under the terms and conditions of the Creative Commons Attribution (CC BY) license (<https://creativecommons.org/licenses/by/4.0/>).

1. Introduction

Ancient mural paintings, found in a multitude of cultures across the globe, hold invaluable cultural and historical significance, making their preservation and analysis of paramount importance. Due to their aesthetic beauty and artistic expression, Roman wall paintings have long fascinated scholars and the general public alike. These ancient artworks offer unique glimpses into Roman life, culture, and artistic techniques; the intricate details and vibrant colors of these mural decorations provide valuable insights into the society and values of the time. Through these paintings, one can appreciate and admire the craftsmen's technical know-how and understand the aesthetics that were prized in ancient Roman society [1]. It is well known that Romans employed painting to create illusions, simulating luxurious building interiors. Wall painting decorations were typically commissioned and served to advertise social ambitions, the wealth and status being expressed in private residential building projects [2,3].

Since the pioneering studies conducted by Jean-Antoine Chaptal and Sir Humphry Davy in the early 19th century [4,5], Roman wall paintings have been the subject of extensive scientific research. These studies have been driven by the desire to understand the materials and painting techniques employed by ancient artists (the exact pictorial technique the Romans used has long been debated), as well as to determine appropriate conservation treatments for these delicate painted surfaces [6,7].

Currently, there is a substantial corpus of data on wall painting supports and pigments, particularly from Rome and Pompeii [1,3]. Wall painting fragments discovered in other parts of the empire, including Northern Italy [8], Spain [9], France [10], Switzerland [11], Great Britain [12], Greece [13], Cyprus [14], Ukraine [15], and Slovenia [16], have also been studied, though to a lesser extent. This lack of systematic analysis concerning Roman wall painting findings is particularly pronounced in the case of the frontier provinces of the Roman Empire, such as Dacia.

A province of the Roman Empire from 106 to 271–275 AD, Dacia, also known as Dacia Traiana or Dacia Felix, covered much of the historical region of Transylvania (modern north-central and western Romania). In contrast to other Roman provinces, Dacia has very few preserved examples of Roman wall paintings. This situation can be attributed to various factors, including environmental/burial conditions, methods of recovery, subsequent conservation treatments (if any), and, not least, historical aspects [17,18]. Unlike the western part of the Roman Empire, where the wall painting technique was a well-established tradition, in Dacia, this artistic phenomenon was not as prevalent. According to existing historical sources, craftsmen with high technical skills and expertise were brought from other provinces specifically for commissioned works [19,20]. Ancient written sources concerning wall painting, including *De Lapidibus* by Theophrastus, *De Architectura* by Vitruvius, and *Historia Naturalis* by Pliny the Elder, mention the advanced technical skills required to carry out such artworks—from know-how on the technique of execution of the support (the laying of the different coats of plaster, the use of preparatory sketches), to the preparation of pigments, the use of various painting techniques and the process of finishing the paint surfaces [1,3].

Archaeological excavations that report the discovery of Roman mural paintings located in the former territory of the Roman province of Dacia are relatively scarce and not widely known [17]. Important discoveries of Roman mural paintings have been reported so far only in a few archeological sites. These isolated discoveries are often found to belong to richly decorated Roman villas (*domus*) occupied by high-ranking dignitaries and other upper-class figures. Notable examples include discoveries at Apulum [21] and Apulum II [22], at Ulpia Traiana Sarmizegetusa [23], and, more recently, at Rapoltu Mare—La vie [24]. Decorative polychrome paintings on plaster associated with monumental public buildings have been discovered to a lesser extent, such findings being reported only in the case of the Roman amphitheater from Porolissum [25], and, in the case of the Roman baths from Alburnus Maior [26].

In terms of publications, most studies discussing mural painting decorations found in Dacia are primarily archeological excavation reports. Historical and art history studies [19,20] have been published less frequently, especially in recent years, while technical and/or interdisciplinary studies conducted on unearthed mural fragments are even more scarce. With the exception of some early analytical reports mentioned in a couple of studies [25,27], to this date there are only a limited number of scientific publications that investigate the material composition of the pictorial layers and explore the pictorial technology of several 2nd c. wall painting fragments discovered within a *domus* at Ulpia Traiana Sarmizegetusa [28], within the Roman baths at Alburnus Maior [29], and within a Roman villa at Rapoltu Mare—La vie [30].

In this study, we report the results of our most recent investigations carried out on a group of wall painting fragments that have never been studied until now. These fragments were excavated in what is probably the most important Roman archeological site in Dacia—Ulpia Traiana Sarmizegetusa [31], the first city established by the Romans in the northern part of

the Danube. As mentioned earlier, the archeological site at Sarmizegetusa is one of the few locations in Dacia where significant segments of decorative polychrome paintings on plaster were discovered in situ. During the archeological excavations carried out between 1984 and 1986, impressive fragments of mural decorations were discovered in structures belonging to the so-called *Domus Procuratoris* [32,33], the subject of this study. Later on, similar discoveries were also found within different architectural buildings from Sarmizegetusa such as the rooms belonging to the *domus* located under the remains of the temple dedicated to the Palmyra gods, west of Trajan's Forum [23,34,35]. Relatively well preserved, some of these murals can be included in the third Pompeian style due to the use of simple, monochromatic panels, clearly individualized, and the occurrence of vegetal motifs [23].

This study builds upon previous works [28,29] and aims to provide new insights into the painting materials and techniques used by ancient artists in the production of wall paintings within the Roman province of Dacia. In order to preserve the integrity of these rare wall painting fragments and avoid sampling as much as possible, a minimally invasive multi-method approach was considered. Specifically, this study combined an array of non- and micro-invasive techniques that have been recognized as efficient and complementary tools for the characterization and identification of a wide range of painting materials. Portable X-ray fluorescence (XRF) and laser-induced breakdown spectroscopy (LIBS) were employed for the elemental characterization of the samples, including the characterization of the painting stratigraphy [36–39]. Attenuated total reflectance–Fourier transform infrared (ATR-FTIR) spectroscopy [40,41] and hyperspectral imaging (HSI) in the short-wave infrared (SWIR) region [42–44] were used to obtain molecular and structural information of the pigmenting materials used for the color palette and to investigate the possible use of organic binders. HSI was also employed to extract enhanced images that could highlight hidden features and concealed details that were not visible through visual inspection, which could offer additional data on the painting technology and working methods. The obtained results are discussed and compared with previous findings [28,29] to provide a deeper understanding of the painting production methods and the artistic practices within the region.

2. Materials and Methods

2.1. Wall Painting Samples

In this study, a group of ten wall painting fragments excavated at Ulpia Traiana Sarmizegetusa archeological site have been examined (Table 1). The samples, never investigated before now, were discovered as loose fragments during excavations conducted between 1984 and 1986, in what appears to have been the *Domus Procuratoris*—the residence of a high-ranking official, the procurator of the province [45–47].

Table 1. Description of the wall painting fragments investigated in this study.


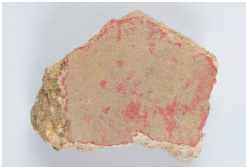

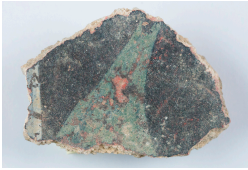

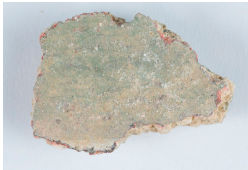




Notation	Photograph	Fragment Description	Painting Materials Identified (Combined Methodology)
S1		Paint layer's hue: green, dark brown Superimposed layers: yes <i>Intonaco</i> layer: - <i>Sinopia</i> : yes, reddish-brown Dimensions (cm): 4.7 × 3.9 × 1.2	Green earth (celadonite), ochre pigment, protein binder, dark-blue undercoat based on calcite admixed with carbon black (soot/charcoal), red ochre (<i>sinopia</i>)
S2		Paint layer's hue: light red Superimposed layers: no <i>Intonaco</i> layer: yes <i>Sinopia</i> : - Dimensions (cm): 2.8 × 2.5 × 0.9	Red ochre (hematite)

Table 1. Cont.

Notation	Photograph	Fragment Description	Painting Materials Identified (Combined Methodology)
S3		Paint layer's hue: yellow, purple-gray Superimposed layers: yes <i>Intonaco</i> layer: yes <i>Sinopia</i> : - Dimensions (cm): 3.7 × 2.4 × 1.9	Yellow ochre (goethite), lead-based pigment mixed with indigo (?), protein binder
S4		Paint layer's hue: green, black, light-blue Superimposed layers: yes <i>Intonaco</i> layer: - <i>Sinopia</i> : yes, dark red Dimensions (cm): 3.7 × 3.1 × 1.4	Green earth (celadonite), amorphous carbon black (soot/charcoal) admixed with ochre, lazurite mixed with indigo (?) and calcite, protein binder, red ochre (<i>sinopia</i>)
S5		Paint layer's hue: deep red Superimposed layers: yes <i>Intonaco</i> layer: yes <i>Sinopia</i> : - Dimensions (cm): 3.4 × 2.3 × 1.1	Red ochre (hematite)
S6		Paint layer's hue: bluish-green, light-blue Superimposed layers: yes <i>Intonaco</i> layer: - <i>Sinopia</i> : yes, dark red Dimensions (cm): 2.3 × 1.6 × 0.8	Green earth (celadonite) admixed with Egyptian blue and yellow ochre (goethite), protein binder, dark-blue undercoat based on calcite admixed with carbon black, red ochre (<i>sinopia</i>)
S7		Paint layer's hue: light-green Superimposed layers: yes <i>Intonaco</i> layer: yes <i>Sinopia</i> : - Dimensions (cm): 3.2 × 2.8 × 0.7	Green earth (celadonite)
S8		Paint layer's hue: red Superimposed layers: yes <i>Intonaco</i> layer: - <i>Sinopia</i> : yes, reddish-brown Dimensions (cm): 5.1 × 1.8 × 1.9	Red ochre (hematite), bone black
S9		Paint layer's hue: pink Superimposed layers: no <i>Intonaco</i> layer: yes <i>Sinopia</i> : - Dimensions (cm): 1.2 × 2.6 × 1.2	Red ochre (hematite) admixed with lime white
S10		Paint layer's hue: greyish-green, orange Superimposed layers: yes (?) <i>Intonaco</i> layer: yes <i>Sinopia</i> : - Dimensions (cm): 4.2 × 2.2 × 1.1	Ochre admixed with carbon black (soot/charcoal), yellow ochre (goethite) inclusions

Note: For each wall painting fragment, the dimensions are given as length × width × depth in centimeters (cm).

Following excavation, the wall painting fragments were not subjected to any restoration or conservation treatments. As a result, the samples retained their original integrity, offering an unaltered view of their authentic characteristics. Of relatively small size, the investigated fragments have relatively well-preserved paint layers in one or more chromatic shades (including superimposed paint layers). Red, pink, yellow, green, purple, blue, brown, and black pictorial layers can be observed in various hues. The support consists of single or two distinct plaster layers (arriccio and intonaco), and some of the samples show evidence of a preparatory drawing made with red paint (*sinopia*) [2,3]—see Table 1 and Figures 1 and S1 (Supplementary Materials). The investigated samples were carefully chosen to be as representative as possible. They reflect the full spectrum of all documented colors and features, ensuring a comprehensive overview of the wall paintings excavated within this particular site. A detailed description of the investigated fragments is given in Table 1.

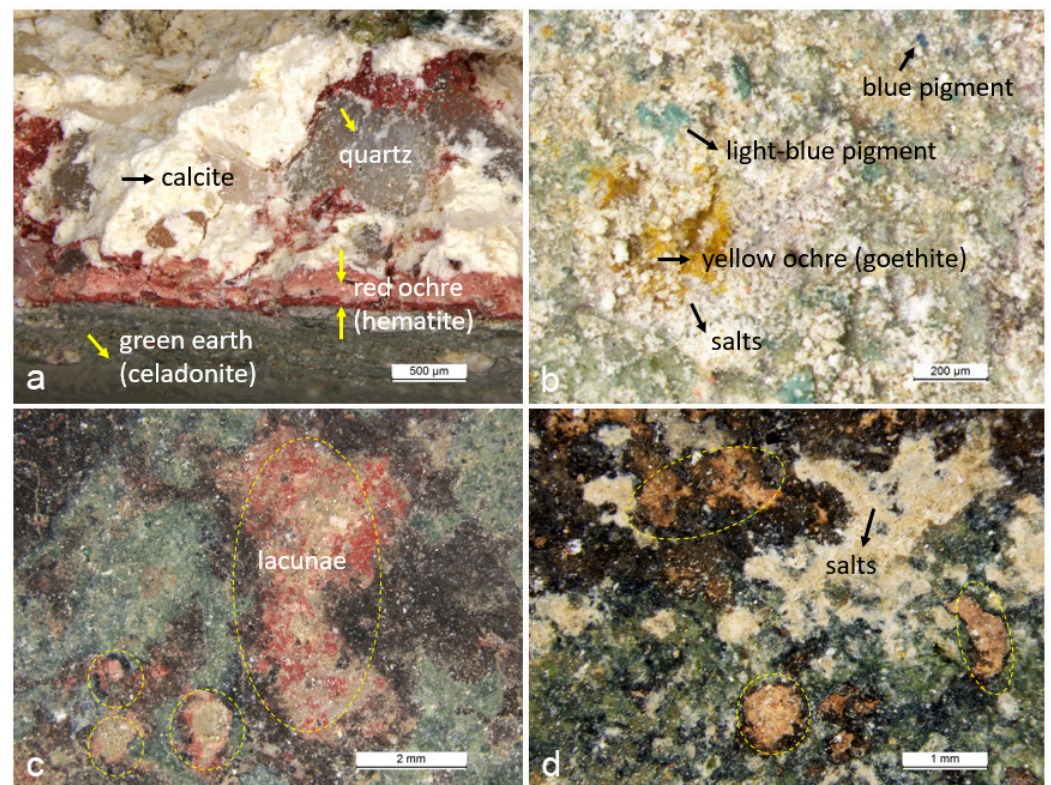


Figure 1. Optical microscopy images that highlight the stratigraphy of the paint layers—sample S6 (a); traces of a richer color palette—sample S6 (b); degradations of the pictorial layers—loss of the original pictorial layers, lacunae (highlighted with yellow dot circles), and formations of salts—sample S4 and S1 (c,d). The presence of a red ochre-based layer underneath the top paint layers was found in some of the investigated wall painting fragments (a,d), and can be linked with the existence of a preparatory drawing (*sinopia*).

All wall painting fragments have been investigated using XRF, ATR-FTIR, and HSI. Additionally, LIBS was carried out specifically on areas with unresolved questions and/or to verify the presence of certain materials that could not be confirmed by other employed techniques. Except for ATR-FTIR analysis, which was conducted on powder samples, all other analytical measurements were performed in situ, without sampling, based on the capabilities of the portable equipment employed. In order to obtain a morphological characterization of the samples, optical microscopy was performed on the wall painting fragments using a Leica M205 FA (Wetzlar, Germany) fluorescence stereomicroscope.

2.2. X-ray Fluorescence (XRF)

XRF measurements were performed with portable, handheld XRF equipment (TRACER III-SD) from Bruker (Billerica, MA, USA). The equipment has an Rh-anode and a 10 mm² silicon drift detector, with 145 eV at a 200,000 cps (Mn K_α line) energy resolution and increased accuracy, down to the ppm level, as a function of the sample's features, and has a spot size of 3 × 4 mm. The experimental parameters were set so as to obtain the best detection accuracy in terms of X-ray intensity and spectral profile across a larger spectral range at a ~11 μA current intensity, a 40 kV tube voltage, a 30 s live time, without filtering of the beam, and under an air atmosphere. Before each measurement session, the instrument's accuracy was checked using a Duplex 2205 check sample, a metal alloy, which contains known concentrations of nickel, molybdenum, chromium, iron, manganese, and other trace metals. Elemental identification was performed using the ARTAX software (v7.4), and data plotting was carried out using Microsoft Excel 2021 and OriginPro 2021b.

2.3. Laser-Induced Breakdown Spectroscopy (LIBS)

LIBS measurements were performed using a handheld Z-Series analyzer from SciAps (Woburn, MA, USA) that employs a YAG:Nd Q-switched laser emitting at the fundamental wavelength of 1064 nm, with the following laser parameters: a spot diameter of 50 μm, an energy of 5 mJ and a 10 Hz repetition rate. The system's CCD spectrometers cover a spectral range from 190 nm to 950 nm. The acquisition is performed in an Argon-purged environment, and the spectral data were collected for targeted analysis using a single-pulse mode in a series of 10 to 25 pulses depending on each area's characteristics. Data processing was performed using Microsoft Excel 2021 and OriginPro 2021b.

2.4. Fourier Transform Infrared Spectroscopy (FTIR)

FTIR spectra were recorded on powder samples in attenuated total reflection (ATR) mode on microsamples, using a Perkin Elmer SpectrumTwo FTIR spectrometer (Waltham, MA, USA) equipped with a Pike Technologies GladiATR accessory (monolithic diamond crystal, 3 mm diameter) (Fitchburg, WI, USA). Small amounts of samples were taken from research interest areas by gently scrapping the surface. Spectra were collected in the 4000–380 cm⁻¹ mid-infrared spectral region at a 4 cm⁻¹ resolution using 32 scans. Data processing was carried out in Essential FTIR (v3.50).

2.5. Hyperspectral Imaging (HSI)

The hyperspectral data acquisition was performed using a portable HySpex SWIR-384 system produced by Norsk Elektro Optikk (Oslo, Norway). The camera features a state-of-the-art Mercury Cadmium Telluride (MCT) detector and is equipped with a cryogenic cooling system, which ensures a constant temperature at 147 K. These characteristics enable low background noise, a high dynamic range, and an optimal signal-to-noise level at a maximum speed of 450 fps. The system, which operates between 950 and 2500 nm, covers parts of the near-infrared (NIR) and short-wave infrared (SWIR) spectral region and it records simultaneously 288 different spectral bands, with a spectral sampling of 5.45 nm. For data acquisition, a 30 cm working distance close-up lens was used in order to provide the best available resolution. Diffuse illumination was provided by two custom-made lamps (T3 halogen incandescent light bulbs R7S) that provide a light output of 2500 lumens and a proper excitation source in the range covered by the hyperspectral camera detector. Radiometric calibration of the SWIR data was carried out using the Hypspec RAD software (v.3.1.), thus converting the digital number (DN) in at-sensor absolute radiance values (W/sr·nm·m²) by using a scaling factor included in the header file. The conversion of the radiance to apparent reflectance was made using the QUAC (QUick Atmospheric Correction) module in ENVI (v.5.3.). A Zenith Lite Diffuse Reflectance Target (50% R) from SphereOptics (Herrsching, Germany) was used as a reflectance standard. Two supervised classification algorithms, Spectral Angle Mapper (SAM) and Linear Spectral Unmixing

(LSU), were applied in ENVI (v.5.3) to the registered hyperspectral data with the aim of clustering similar pigments (or pigment mixtures) and mapping their distributions.

3. Results

3.1. XRF Analysis

Due to the non-destructive nature of the measurements and the features of the wall painting fragments, which are layered, inhomogeneous materials, sometimes showing surface depositions, XRF analysis has been carried out on multiple areas of each given sample. Given the working protocol employed, the obtained XRF results can be regarded as semi-quantitative. The identified elements are listed in Table 2, based on their relative contribution to the overall spectrum: major—defined as the main elements detected; minor—defined as the peaks ten times lower than the major peaks; and trace—defined as all other detected elements above the detection limit. The table excludes elements that were identified but fell below the calculated detection limit (Na and Mg were not detected above the LOD in any of the analyzed samples).

Table 2. Results of the XRF analysis. Identified elements are shown in order of decreasing abundance.

Sample Area	Description	XRF-Detected Elements		
		Major	Minor	Trace
S1-1	Brown paint layer	Ca, Fe	Sr	K, Zr, Mn, Ti, Si, Rb, Pb, Cu, P, Zn, S
S1-2	Green paint layer	Ca, Fe	K, Sr	Zr, Ti, Mn, Si, Pb, Cu, P, Zn, Cr, S
S1-3	Lacuna (<i>sinopia</i>)	Ca, Fe	Sr, K	Ti, Mn, Si, Zr, Rb, Pb, Cu, P, S, Zn, Al
S1-4	Substrate/mortar	Ca, Fe	K	Sr, Ti, Si, Mn, Rb, Zr, Pb, Cu, Zn, S, P, Cr
S2-1	Red paint layer (with depositions)	Ca, Fe	As	K, Sr, Si, Ti, Pb, Mn, Cu, S, Al, Zn
S2-2	Red paint layer	Ca, Fe	As	K, Sr, Si, Ti, Pb, Mn, S, Cu, P
S2-3	Substrate/mortar	Ca, Fe	K	Si, Sr, Ti, Zr, Mn, Rb, Cu, Pb, Ba, S, Al, P
S3-1	Yellow paint layer	Ca, Fe	-	K, Ti, Si, Sr, Mn, Pb, Zr, Rb, Cu, S, Zn
S3-2	Purple-gray paint layer	Ca, Fe	Pb	K, Ti, Sr, Si, Mn, Zr, Cu, Rb, Zn, Al
S3-3	Substrate/mortar	Ca, Fe	K	Sr, Ti, Si, Mn, Zr, Rb, Pb, Cu, Ba, Cr, S
S4-1	Black paint layer	Ca, Fe	-	As, Sr, Si, K, Mn, Ti, Pb, Cu, S, Ba, Zn
S4-2	Green paint layer	Ca, Fe	K	Si, Sr, As, Ti, Mn, Pb, Cu, Zn, S, P
S4-3	Lacuna (<i>sinopia</i>)	Ca, Fe	-	K, Si, Sr, As, Ti, Mn, Pb, Cu, S, P
S4-4	Substrate/mortar	Ca, Fe	-	K, Si, Ti, Sr, Mn, Zr, Rb, Cu, Pb, S, P, Al
S4-5	Light-blue paint layer	Ca, Fe	-	K, Sr, Pb, Si, Mn, Ti
S5-1	Red paint layer	Ca, Fe	As	Sr, Si, K, Ti, Mn, Pb, S, Cu, Rb, P, Al
S5-2	Substrate/mortar	Ca, Fe	K	Sr, Ti, Si, Rb, Zr, Mn, Cu, Pb, Cr, P, S
S6-1	Light-green paint layer	Ca, Fe	K	As, Sr, Si, Ti, Pb, Mn, Cu, S, Zn, Al
S6-2	Substrate/mortar	Ca, Fe	K	Sr, Ti, Si, Mn, Zn, Cu, Al, Pb, Cr, P, S
S7-1	Green paint layer (with lacunas)	Ca	-	K, Sr, Ti, Si, Zr, Mn, Rb, Cu, Pb, S, Zn, P, Cr
S7-2	Green paint layer (with depositions)	Ca, Fe	K	Sr, Ti, Si, Mn, Zr, Rb, Cu, S, P, Pb, Al, Zn, Cr
S7-3	Green paint layer	Ca, Fe	K	Sr, Ti, Si, Zr, Mn, Rb, Cu, Pb, Zn, S, Al
S7-4	Substrate/mortar	Ca	Fe	K, Sr, Ti, Si, Zr, Mn, Rb, Pb, Cu, Zn, S, Al
S8-1	Red paint layer	Fe, Ca	Sr, As	Pb, K, Ti, Si, Zr, Mn, Rb, Zn, Cu, S, Cr, Al
S8-2	Substrate/mortar	Ca	Fe	K, Sr, Ti, Si, Mn, Rb, Pb, Zr, Cu, S
S9-1	Pink paint layer	Ca	Fe	Sr, K, Ti, Si, Rb, Zr, Mn, Pb, Cu, Zn, S
S9-2	Substrate/mortar	Ca	Fe	K, Sr, Ti, Si, Mn, Zr, Cu, Rb, Pb, S, Zn, Ba, Cr
S10-1	grayish-green paint layer	Ca, Fe	Si	K, Ti, Sr, Mn, Pb, Cu, Zr, S, Cr, Rb, Zn, Al, P
S10-2	Yellowish orange paint layer	Ca, Fe	-	K, Ti, Mn, Sr, Cu, Pb, Zr, Al, S, Rb, P, Zn
S10-3	Substrate/mortar	Ca	Fe	K, Si, Sr, Zr, Ti, Mn, Rb, Ba, Cu, Pb, Zn, S, Al, P

As can be seen in Table 2, calcium and iron were the dominant elements detected within all areas. The high calcium content primarily originates from the preparation layer (observed in some of the samples), as well as from the mortar base and possibly from the use of a lime-based binder. Given the low levels of sulfur detected, the presence of secondary gypsum (as superficial alteration product) can be excluded [48]. Strontium, a substitute of

calcium in both calcite and aragonite [49], is also present in small amounts across all the investigated areas and can be linked with the presence of calcium-based minerals.

Figure 2 shows the distribution of three of the detected elements (iron, arsenic, and lead) across all analyzed areas. The corresponding net count rates recorded for each analysis area were normalized with respect to the Rh $K\alpha$ line in order to allow for semi-quantitative analysis. Iron, one of the main elements present in all registered XRF spectra, is likely associated with the constituent chromophore phases (mixture of ferric oxo-hydroxide minerals) of the various earth-based pigments dispersed in the paint layers as well as in the red-colored preparation layer [50,51]. As easily observed in Figure 2a, the highest levels of iron were identified on the red-pigmented areas in sample S5 and sample S8, which infers the use of an iron-rich red ochre [2,3,52]. The use of yellow ochre can also be inferred, as indicated by the high iron level registered on the yellow paint layer in sample S3. Additionally, some of the green areas (S4-2 and S6-1) also showed notable iron levels, probably due to the use of green earth (terra verte). This hypothesis is also sustained by the slightly higher levels of potassium registered for the green chromatic areas, indicative of potassium-rich minerals, such as celadonite and glauconite, which are typically found in green earths [53].

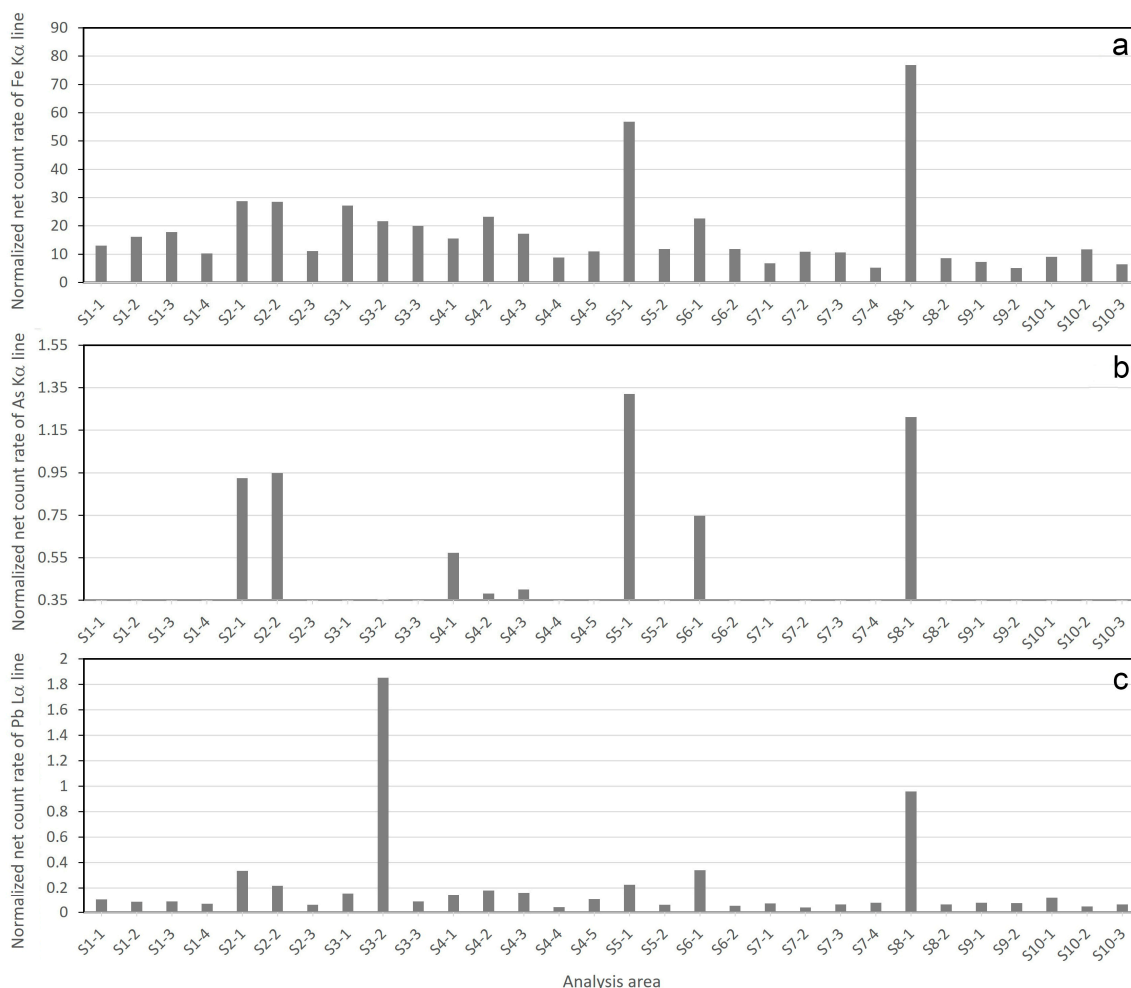


Figure 2. Normalized net count rate distribution of iron (a), arsenic (b), and lead (c) levels throughout all analyzed areas.

The presence of several trace elements has been highlighted in the XRF spectra. Some of them, such as Sr, Ti, Al, S, and P could be related to the calcium-based matrix [54], but given the low correlation between calcium and these trace elements (see Figure 3), this

does not seem very plausible. More likely, such trace elements are terrigenous markers linked to the burial environment or to the geological origin of the pigments [55–57]. Other elements, including Si, Al, Ti, Mn, As, Pb, Cu, and Zn, can be likely associated with the silicate-based accessory phases of the earth-based pigments [53], widely used across the wall painting fragments investigated. However, the detection of significant amounts of certain transition metals and metalloid elements, such as lead and arsenic, may suggest the presence of additional pigmentation compounds. Arsenic lines have been evidenced in several red areas (S2-1, S5-1, S8-1), as can be seen in Figure 2b, identified through the presence of both $K\alpha$ and $K\beta$ lines (Figure S2). Looking at the correlation matrix (Figure 3), it can be seen that iron and arsenic are positively correlated ($r=0.84$), suggesting that they come from a common source.

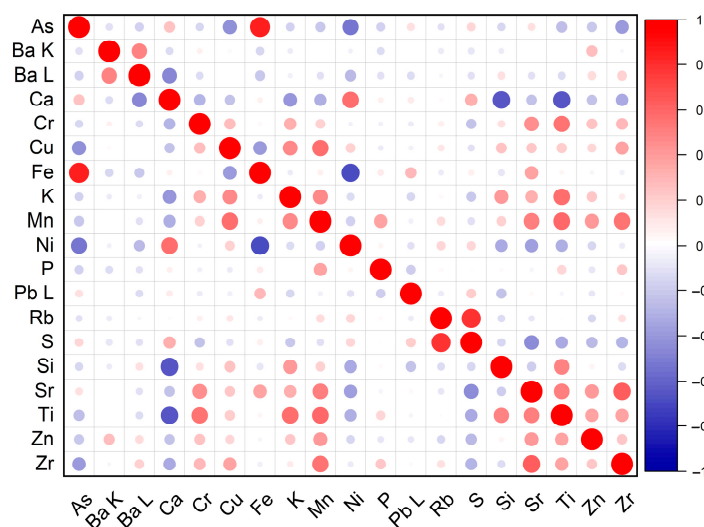


Figure 3. Pearson correlation matrix.

The presence of arsenic, one of the most frequently encountered impurities in iron ores, with common occurrences being arsenopyrite and its weathering products [58], can be related to the extraction source of the earth pigments [57]. As evident in Figure 2b, arsenic traces were also registered on the samples displaying a red preparation layer/sinopia (S4, S6), which can infer the idea that the same red ochre was used for the top red-colored layers.

Significant levels of lead have been registered on the purple-gray paint layer (S3-2) as well as on the red paint layer in sample S8 (Figure 2c). Similar to arsenic, lead is also a naturally occurring impurity in ochre-based pigments, both elements having a tendency to be adsorbed through surface interaction onto phyllosilicates and transition metal oxides [59,60]. However, in this case, the intensity of the lead lines is much higher (compared to the other areas), suggesting the intentional addition of a lead-based pigment, in order to obtain the desired shades. As documented in various historical sources, several artificial lead-based pigments (like, for example, lead white, minium, and massicot) were known and employed by the Roman artists, alone or admixed with other pigments, such as ochres [61]. Taking into account the purple shade of the investigated area, one possibility would be the use of a mixture based on lead white and Tyrian purple, a shellfish-derived pigment [62]. However, considering the high cost of this pigment [52], it is less likely that such a mixture was employed. Instead, more accessible violet pigments may have been considered such as a reddish-purple created by heat treatment of hematite (known as caput mortuum, usta, or ostrum) [63], a mixture of Egyptian blue with red ochre [64] or with red lead (minium) [65], a mixture of green earth and hematite [65], or a mixture of organic dyes madder and indigo [66]. According to existing sources, another method to create purple hues involved applying cinnabar on top of an indigo layer [67]. From the above-mentioned hypotheses, based on the low levels of copper registered for this area, we can exclude

the presence of Egyptian blue (a copper calcium silicate). The use of cinnabar can also be ruled out, as no Hg lines were registered. The other hypotheses will be evaluated through complementary techniques, as discussed in the following sections.

For the black-pigmented area investigated (S4-1), a mixture of ochre and carbon black pigments can be inferred, with such mixtures being frequently reported in the literature, charcoal being added to enhance the opacity of the relatively transparent ochre pigments [50].

As observed in the macroscopic images registered on the surface of some of the investigated wall painting fragments, traces of a richer color palette can be seen, as, for example, sample S6 (Figure 1b), where various blue-colored particles and yellow paint spots can be easily observed on top of the light-green paint layer. Due to the limitations of the handheld XRF equipment, which has a spot size of 3×4 mm, such small particles and/or colored areas cannot be analyzed individually, and micro-analytical techniques are required. In this particular case, the bluish-green hue may have been obtained by mixing green earth with small quantities of Egyptian blue and yellow ochre, a practice documented in several other studies [68–70]. The blue- and yellow-colored grains still present on the surface could also be associated with the existence of a superimposed paint layer (on top of the light-green background) which, over time, has been lost. The existence of more complex decorative patterns and/or the use of pigment mixtures can also be inferred for several other fragments, as highlighted in Figure S1.

The visual examination of the coarse plaster layers (arriccio) shows a very heterogeneous composition made of various aggregates, including visible lumps of calcite, quartz, and ochre pigments. The presence of ochre nodules in the mortar indicates the use of local material, such as river sand with impurities, and explains the minor Fe input registered in these areas. These ochre inclusions could also result from the manufacturing process of the raw painting materials, such as the use of the same tools when preparing the mortar and the pigments. In terms of trace elements, the average concentrations of Zn and Rb are notably higher in the mortars compared to the painted areas, likely related to the type of aggregate used [71].

3.2. LIBS Analysis

To obtain further elemental information, including stratigraphic analysis of the investigated wall painting fragments, and thus overcome some of the limitations of the XRF measurements—such as low detection limits for light elements, shielding and layering effects [72]—LIBS analysis was considered. Due to its micro-destructive nature and the high historical value of the wall painting fragments, LIBS measurements were carried out only on fragments S4 and S6 that show the existence of several paint layers and/or the presence of the red preparatory drawing (*sinopia*). The stratigraphic results provided by LIBS on selected areas are shown in Table S1 (see Supplementary Materials).

In alignment with the recorded XRF data, Ca and Fe are among the primary elements identified via LIBS across all the examined areas. Cu, Pb, C, Sr, Ti, Cr, Al, Na, Mg, Mn, K, and Si were also detected in minor or trace amounts. Due to the presence of related mineral components rich in iron oxides and aluminosilicates, the chemical fingerprints registered in the areas analyzed using LIBS are relatively similar. Nonetheless, by correlating the distribution of elements with the LIBS depth profile and their relative abundances in the spectra, the emerging patterns align well with the paint layer stratigraphy as observed under microscopic examination, providing additional insights. Figures 4 and 5 depict the distribution of the main elements of interest—Cu, K, Sr, Fe, Al, Pb, Si, and C—throughout the LIBS stratigraphy. As observed in Figure 4a, which corresponds to a lacuna exposing the red underlayer on sample S4, the first laser pulse detects lower levels of Fe and Al on the exposed surface, alongside higher concentrations of Pb. However, from the second pulse onward, Pb diminishes as Fe becomes more predominant. The greater abundance of lead on the surface of the lacuna may indicate the presence of a lead-based pigment on top, related to the black paint layer for which a pigment mixture was most probably used.

These results are in agreement with the XRF data and sustain the hypothesis that some types of lead-based pigment have been used to obtain the desired hue or to enhance the specific properties of the painted surface [50,61].

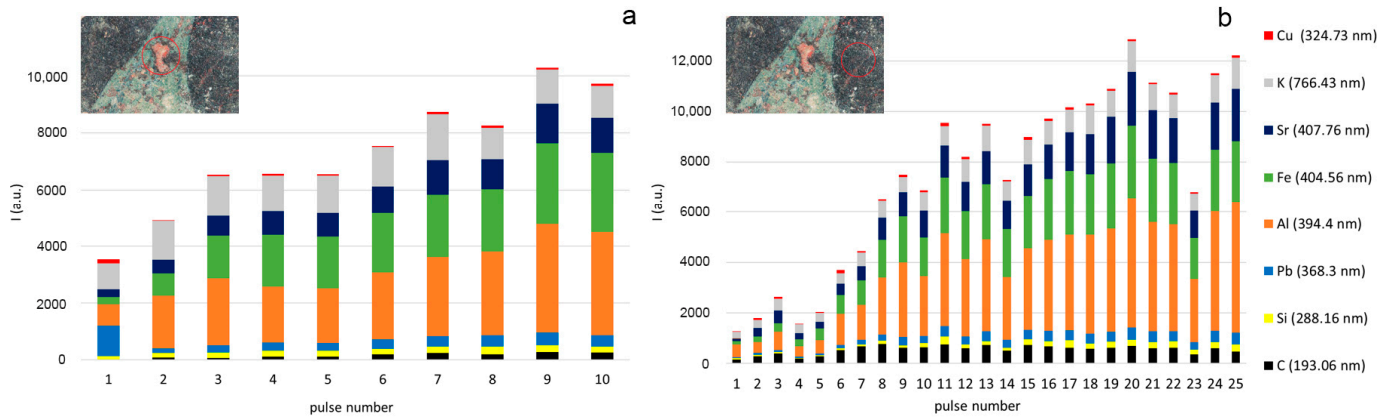


Figure 4. LIBS stratigraphic distribution of the main elements of interest on the red lacuna area (a) and on the black paint layer (b) on sample S4. The emission lines are labeled on the right side of the image.

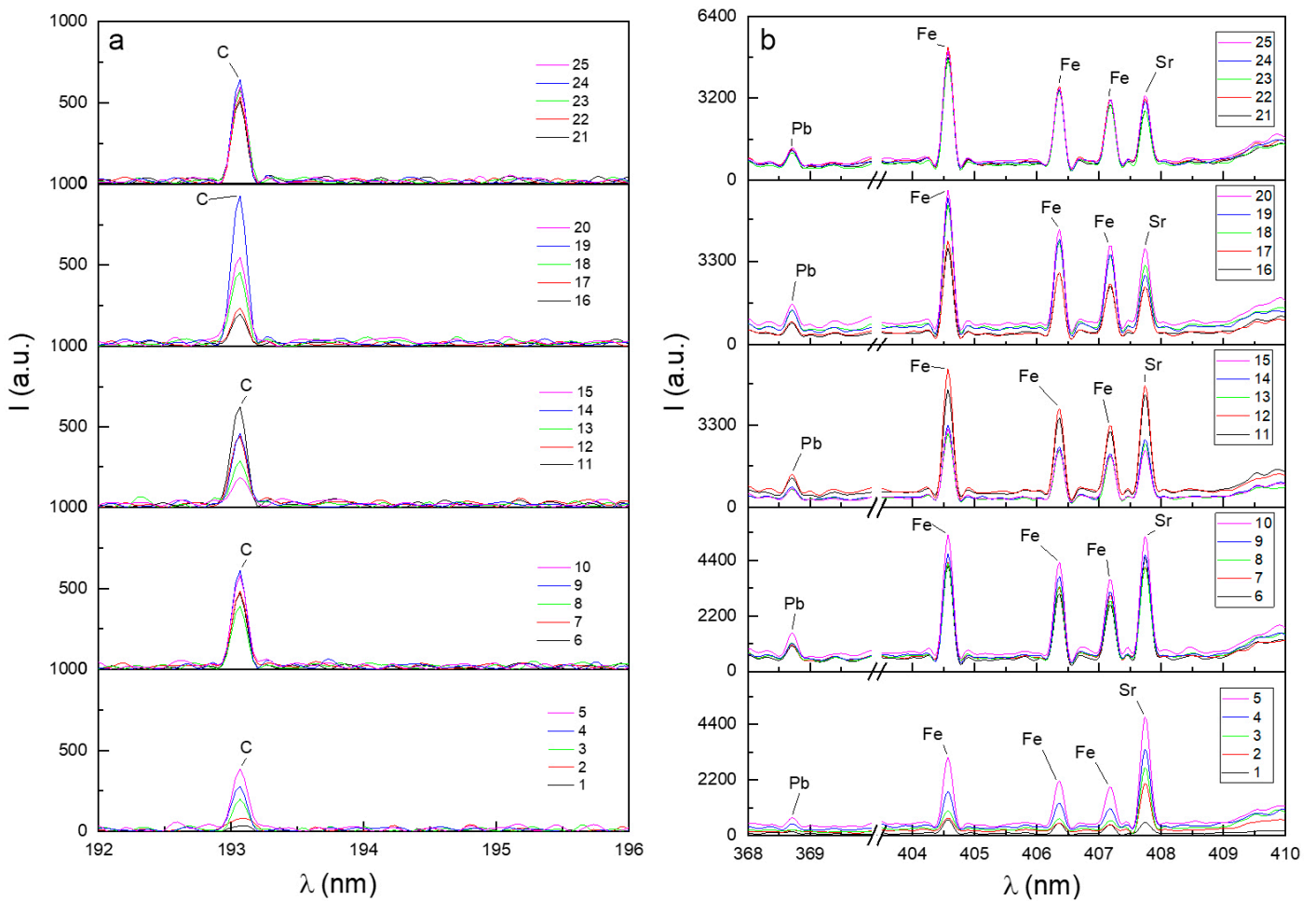


Figure 5. LIBS stratigraphy analysis on sample S6: C peak (a), Pb, Fe and Sr peaks (b).

In the LIBS data recorded for the black-painted area on sample S4 (Figure 4b), a significant difference is observed in the first five pulses, where the relative abundance of the

identified elements is notably low, suggesting the presence of organic components—either related to the presence of an organic dye or to the use of an organic binder. Furthermore, for the same area, the abundance of carbon species is higher starting with pulse seven, suggesting that a black carbon-based pigment is present (admixed with an iron-rich ochre) [39,50]. While the iron abundance collected at different depths remains relatively stable, starting with pulse twenty-three, a transition occurs to another layer, likely indicating that the laser pulse has reached the red preparatory layer underneath the top black layer. For the light-blue paint layer in sample S4, higher abundances of Mg were registered, suggesting the idea that perhaps dolomite was added as a whitener [39].

LIBS data obtained on the bluish-green paint layer on sample S6 could not confirm the presence of Egyptian blue, an artificial copper calcium silicate pigment inferred via microscopic examination and historical sources. Copper was identified only as a trace element with a low spectral abundance. These results could be explained by the fact that the laser spot did not hit the Egyptian blue pigment particles, which are unevenly dispersed within the top paint layer, as observed under microscopic examination. For the same area, the elemental distribution profile for pulses thirteen to seventeen (as shown in Figure S3) suggests the existence of an intermediate layer, which, based on the microscopic observations (Figure S1b), can be linked with a dark-blue undercoat. As shown in Figure 5a, the carbon peak reaches a maximum in the spectra collected at intermediate depths. For the same area, the iron content is lower only during the first five laser pulses, after which it begins to increase and remains relatively constant (Figure 5b). The in-depth iron distribution suggests that iron-rich pigments are present within this intermediate layer as well (iron oxides are also present in the top paint layer, and in the red *sinopia* layer, hence the constant Fe signal). Based on the registered data, it is likely that this undercoat consists of calcite mixed with carbon black and some iron oxides, a mixture typically employed to obtain an optical blue hue [73]. This hypothesis was confirmed via combined FTIR analysis and hyperspectral imaging, as further discussed in Sections 3.3 and 3.4.

3.3. FTIR Analysis

As expected, and in accordance with the obtained elemental data, the FTIR spectra registered on all pigmented layers are characterized by the presence of strong calcite peaks related to the carbonation process and, to a certain degree, to the lime with which the pigments were mixed to obtain the desired hues. The characteristic absorptions associated with calcite (CaCO_3) can be observed at $\sim 1400\text{ cm}^{-1}$ (broad band ascribed to the ν_3 anti-symmetric stretching), 872 cm^{-1} , and 712 cm^{-1} (sharp peaks ascribed to the ν_2 out-of-plane bending and ν_4 in-plane bending). The small peaks at 2512 and 1796 cm^{-1} (combination bands), visible in some of the registered spectra, are also attributed to calcite [29].

FTIR measurements on the red-pigmented areas (samples S2, S5 and S8) clearly revealed the use of a red iron oxide pigment, with characteristic bands for hematite (Fe_2O_3) being observed around 531 cm^{-1} and 467 cm^{-1} (ascribed to lattice vibrations) [53]. Among the various red pigment samples analyzed, the position of the first band (associated with hematite) ranges from 531 to 536 cm^{-1} , while the position of the second band remains unchanged but is generally more intense, which indicates that the hematite particles are platy or elongated [74]. Previous studies have shown that the position and shape of these bands vary according to the size and shape of the hematite particles [75], characteristics that can be linked to different pigment sources and/or various processing methods. In addition to hematite, the FTIR spectra registered on these samples (Figure 6a) showed strong absorptions associated with the presence of clays from the kaolin group and quartz, common accessory minerals found in red ochres. Kaolinite was identified based on the characteristic peaks observed at $\sim 1030\text{ cm}^{-1}$ (Si-O-Si), 1010 cm^{-1} (Si-O-Al), and 918 cm^{-1} (Al-O-H), with the last two bands typically observed as shoulders. The outer and inner hydroxyl ion bands typically found in kaolinite within the $3700\text{--}3600\text{ cm}^{-1}$ spectral region are very poorly defined and hardly visible in the spectra, indicating that the OH groups' bonding to the kaolinite structures was profoundly modified [76], most likely during

pigment grinding [77]. The characteristic bands for quartz (SiO_2) can be easily observed at 1164, 1080, 798, 779, and 696 cm^{-1} [53]. The use of a red ochre pigment was also confirmed for the red preparation layer in samples S1, S4, and S6.

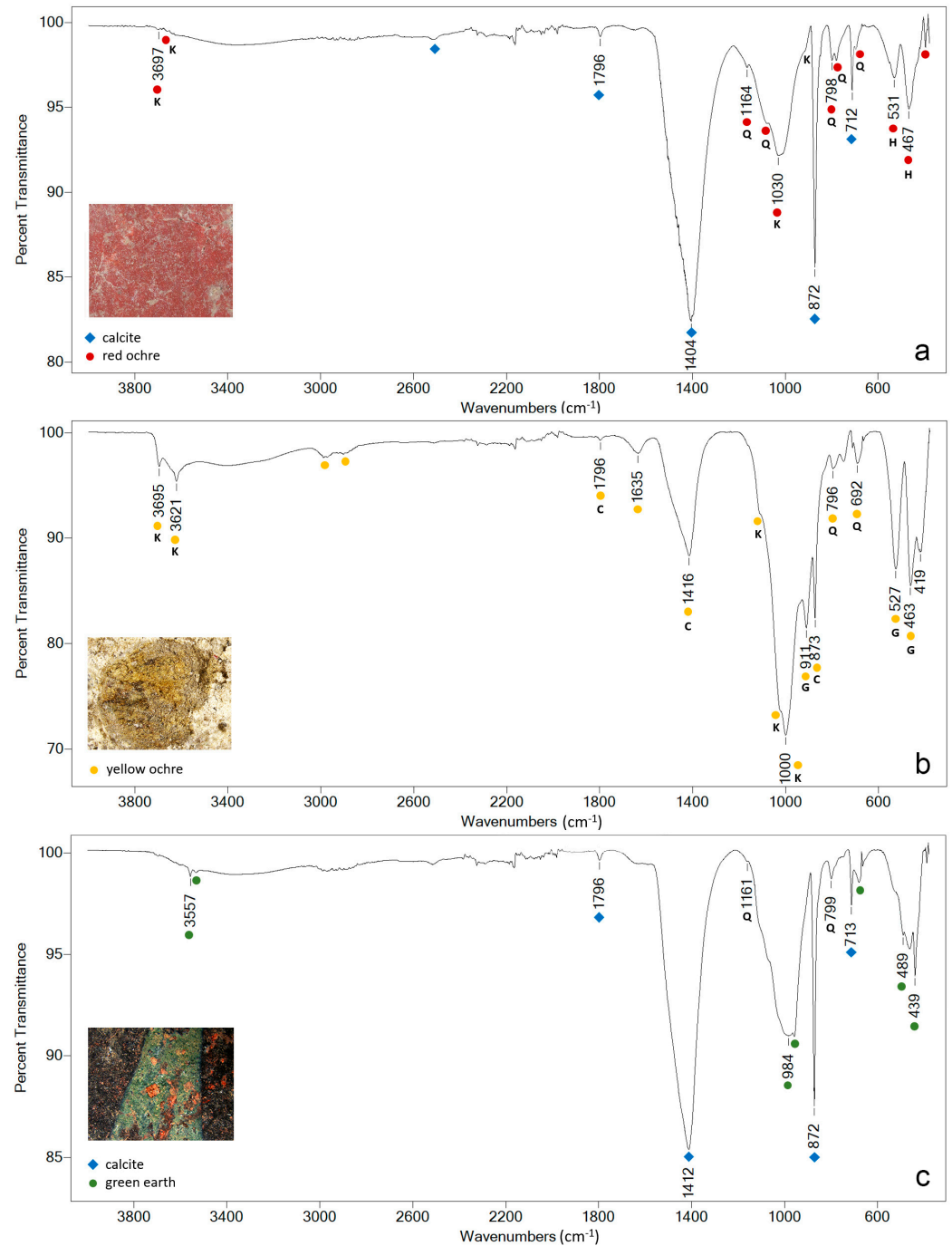


Figure 6. FTIR spectrum registered on the red paint layer on sample S2 (a), on a yellow ochre nodule extracted from the substrate of sample S3 (b), and on the green paint layer on sample S4 (c). The absorptions of the various accessory minerals associated with the natural earth pigments are marked on the spectra as follows: K, kaolinite; Q, quartz; C, calcite; H, hematite; G, goethite.

The FTIR spectrum registered on the yellow-pigmented area (sample S3) shows many similarities with the red ochre's infrared spectrum—strong peaks associated with kaolinite, quartz, and ferric oxide. The characteristic bands for goethite (limonite), the main coloring agent in yellow earths, could not be observed. The hydroxyl stretch at approximately

3150 cm^{-1} is missing, and the hydroxyl deformation bands near 800 and 900 cm^{-1} are masked by the presence of silicates (especially quartz) and other clay minerals [53]. A more refined spectra of the yellow ochre pigment can be seen in Figure 6b, registered on an ochre nodule extracted from the mortar layer of sample S3. As can be easily observed, in this case, the hydroxyl peaks in kaolinite are well defined (peaks at 3695 and 3621 cm^{-1}), and the bands ascribed to (hydrated) ferric oxides are much more intense, and slightly shifted to lower wavenumbers (peaks at 527 and 463 cm^{-1}). Calcite is also present as an accessory mineral within the yellow earth, as indicated by the characteristic peaks registered at 1416, 872, and 712 cm^{-1} . The weak bands between 3000 and 2850 cm^{-1} can be ascribed to aliphatic C–H stretching absorption [78], while the broad band at 1635 cm^{-1} is related to the adsorption of water [79].

The hypothesis of using a green earth pigment derived from a potassium-rich mineral, as inferred from the elemental data, was supported via FTIR analysis. The presence of celadonite could be clearly confirmed via the characteristic bands registered on the green pigmented areas (Figure 6c)—small peaks at 3557, 3534 cm^{-1} (OH stretching), strong band at 958 cm^{-1} (Si–O stretching), with a shoulder band at 1072 cm^{-1} [53]. The broad peak centered around 985 cm^{-1} can be linked with a higher Al tetrahedral substitution, suggesting the presence of lower-ordered type of structures [80]. The hypothesis that Egyptian blue was mixed with green earth to create the lighter green hues, as seen in sample S6, could not be confirmed via FTIR analysis. No distinct diagnostic bands for Egyptian blue are visible, likely due to spectral interferences (overlapping bands), as numerous other painting components present, primarily silicates, exhibit absorption in the same spectral region [81].

FTIR data registered on the purple-gray paint layer in sample S3 revealed similar spectral features as the FTIR data obtained on the yellow ochre paint layer underneath. The spectrum is dominated by strong bands due to calcite. Compared to the yellow-ochre paint layer underneath, the purple paint layer on top displays more intense and broader peaks at 528 and 468 cm^{-1} , ascribed to ferric oxides. Based on the hypothesis derived from the XRF data registered on the same area, the use of caput mortuum admixed with white lead can be ruled out. Compared to red ochre, caput mortuum's IR spectrum is characterized by broader peaks within the fingerprint region that are also shifted to higher wavenumbers values—545 and 473 cm^{-1} [82]. No characteristic peaks for lead white could be observed either—strong and broad band centered at ~ 1400 cm^{-1} , with sharp bands at 1046 cm^{-1} and 680 cm^{-1} [83]. However, the presence of lead white cannot be definitely excluded as the peaks may be hindered by the strong calcite and quartz absorptions that fall within similar regions. The use of an organic dye (indigo) alone or admixed with others (such as madder or safflower red), another hypothesis regarding the employed purple pigment, could not be confirmed via FTIR either. Complementary or more powerful techniques, such as chromatographic methods, are required in this case [67], more so as alteration phenomena and a low concentration of the (presumably present) organic colorants can limit the detection capabilities of FTIR.

However, for the light-blue paint layer of sample S4, indigo could have been used. The FTIR spectrum registered on the sample extracted from this area (Figure 7) shows characteristic peaks around 560, 530, 470, and 420 cm^{-1} (sharp bands), as well as some poorly resolved features (due to the low quantity of the measured sample) around 3700, 1493, 1460, and 1090 cm^{-1} , which could be ascribed to indigo [84]. For the same area, a strong band around 955 cm^{-1} can be observed, which, together with the peaks observed at 892 (shoulder band), 634, and 447 cm^{-1} , may be linked with the presence of lazurite [84]. Compared to Egyptian blue and indigo, lazurite was less common in Roman wall paintings. To date, this pigment has been reported in only a limited number of studies, typically mixed with other pigments to obtain various hues such as dark blues (in admixture with goethite and carbon black) or dark browns (in admixture with hematite and goethite) [85].

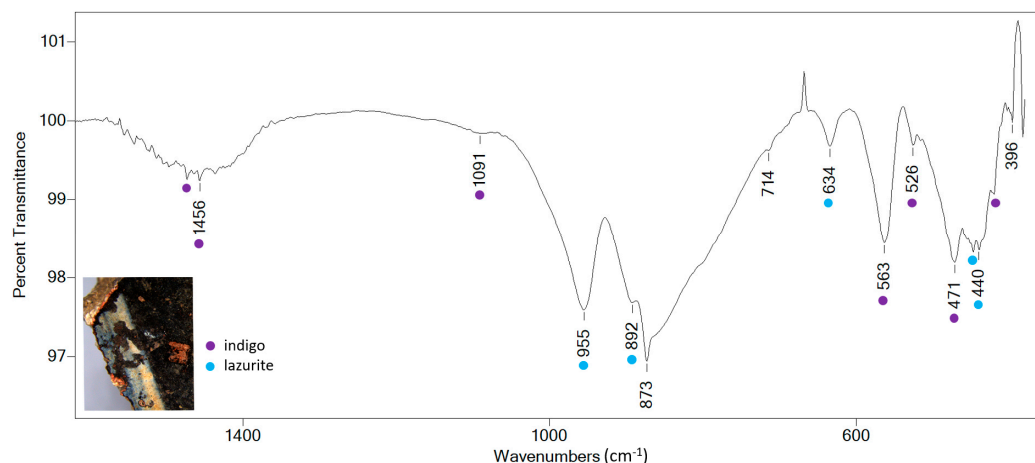


Figure 7. FTIR spectrum (detail within the fingerprint region) registered on the light-blue paint layer on sample S4.

An optical blue—a white pigment (calcite in this case) mixed with carbon black and/or a dark iron-based pigment [73]—may have been used for the dark blue paint underlayer observed in sample S6. The FTIR spectrum for this area shows high amounts of calcite, some silicates, and iron oxides but no characteristic peaks for any blue pigment. According to existing sources, applying such an undercoat can enhance the color intensity of the top paint layer. This practice is documented in the literature, particularly with Egyptian blue, a glassy pigment with low coloring power, which, if applied over a blue or blue-gray undercoat, produces a more vibrant hue [73].

Regarding the black-pigmented areas, the FTIR data obtained supports the hypothesis that a mixture of ochre and carbon black pigments was used [50]. The FTIR spectrum of the black-pigmented sample extracted from sample S4 is characterized by the typical sharp peaks of calcite, along with the characteristic peaks ascribed to an earth-based pigment rich in ferric oxides, kaolinite, and quartz. No other significant spectral features that could be ascribed to the presence of bone and vine black pigments were highlighted in the spectrum [86], suggesting that an amorphous carbon black pigment was used—most probably soot—the main black pigment recommended by Pliny [52].

A bone black pigment might also have been used, as inferred by the characteristic bands ascribed to hydroxyapatite found on a greyish paint layer extracted from fragment S8. The absorption bands at 602 and 563 cm^{-1} (ascribed to P-O bond vibrations), along with the broad peaks centered around 1647 cm^{-1} and 3450 cm^{-1} (ascribed to O-H vibrations), are in agreement with the presence of hydroxyapatite [86,87]. As expected for pigments obtained via bone calcination, strong calcite bands are also registered for this sample. As shown in Figure S4, the calcite peaks are significantly higher than those in the underlying red paint layer, supporting the idea that the calcite contribution in the grayish paint layer is partially due to the use of a bone black pigment.

Related to the possible use of organic binders, ATR-FTIR analysis did not reveal any clear spectral features that may definitively indicate the presence of organic compounds or degradation products of organic binding media. In some of the registered spectra (see Figures S5 and S6) some small, poorly defined, bands can be seen in C-H stretching region (3000–2800 cm^{-1}), as well as in the Amide region—peaks at 1645 cm^{-1} and 1588 cm^{-1} (shoulder)—which is a possible indicator of a protein-based binding media, such as animal glue [41]. The Amide bands are slightly better resolved in the second derivative profile, with the data treatment also revealing the Amide III band around 1460 cm^{-1} (overlapped in the spectra by the strong calcite peak), as well as a small peak around 1248 cm^{-1} that can be ascribed to lipids (C-O bonds). As easily observed, due to the strong contribution of the calcium carbonate matrix, the band intensity of these alleged organic compounds is very weak, making it difficult to clearly identify the presence of organic binders using

FTIR analysis alone. The degradation of the original organic compounds and the low concentration of these species can also add considerable difficulties to their identification, especially when using conventional analytical methods [6,41,88].

FTIR data registered on the intonaco layer (Figure S7) indicate high amounts of calcite admixed with small amounts of quartz, probably derived from river sand. The results obtained on the arriccio layer, composed of lime, siliceous sands, and clay-rich materials, align with previous studies and indicate a regional adaptation [28,29].

3.4. HSI Analysis

SWIR hyperspectral analysis carried out on the investigated wall painting fragments provided additional insights in terms of painting materials and technique, and in some cases, highlighted faded decoration details on the pictorial surface that were no longer visible to the naked eye. As shown in Figure 8, starting with the 1600 nm band, a decorative linear pattern can be easily observed on the surface of sample S6. This detail, although no longer visible on the surface, suggests that originally, this wall painting fragment had a more complex polychromy, with at least two pictorial layers superimposed (on top of the *sinopia* layer). Given the increased absorbance of the (hidden) decorative linear pattern at longer wavelengths, the use of a pigment mixture rich in carbon black could be hypothesized (towards higher wavelengths, the iron/clay pigments become transparent while the black carbon exhibits a high degree of absorption thus becoming visible). As already discussed, the microscopic examination of this area also highlighted the presence of several blue-colored particles, with historical sources suggesting the use of Egyptian blue. For the same fragment, a dark-blue undercoat was also observed in the cross-section, located in the lower region of the sample that still preserves small areas of bluish paint layers (Figure S1b).

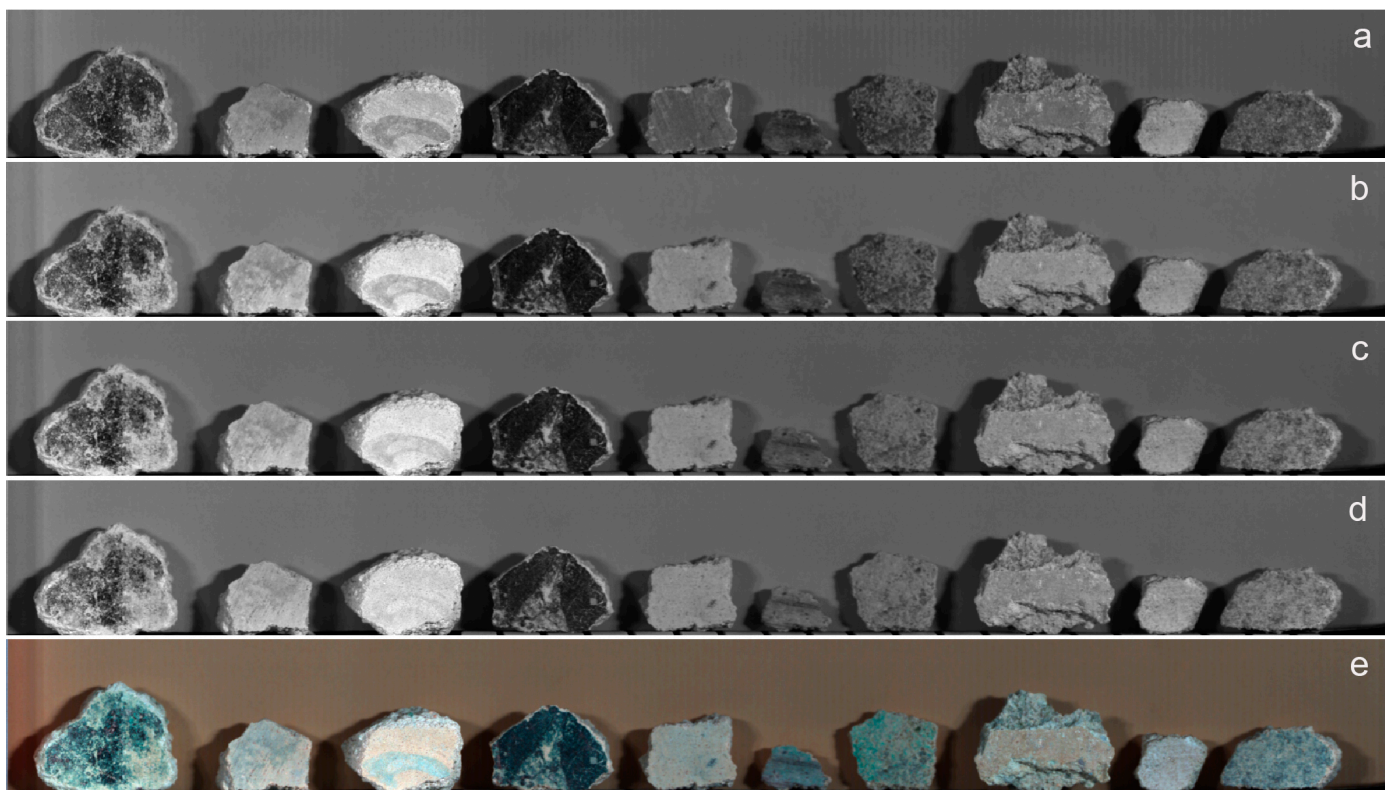


Figure 8. SWIR data that highlight the behavior of the pigmented surfaces at specific wavelengths: 954 nm (a), 1204 nm (b), 1600 nm (c), 2003 nm (d), FCIR RGB: 1367-2182-2459 nm (e). Samples are displayed from left to right (S1 to S10) according to the notations used in Table 1.

Based on the above observations and corroborated by the LIBS stratigraphic data, which highlighted the existence of an intermediate layer in the same region as the decorative pattern observed under HSI, it is most likely that originally, an Egyptian blue paint layer was applied on top of an optical blue underpainting consisting of lime-bound carbon black admixed with some iron-rich ochre, with such practices being documented [73,89]. In other studies, Egyptian blue paint layers were also found to be applied on top of an inner layer of Egyptian blue mixed with celadonite [90]. Given the fact that this pigment is not easy to spread in the *a fresco* technique, the top Egyptian blue paint layer may have been applied *a secco*, with the blue pigment being mixed with an (organic) additive [69,91].

To extract the most meaningful information from the original HSI datasets and obtain distribution maps of the pictorial materials on the surface, the Spectral Angle Mapper (SAM) algorithm in ENVI was used. SAM is a supervised classification method that assesses the similarity between each spectrum associated with the pixels of the imaged area and a reference spectrum (endmember). The algorithm assumes that spectra are represented as vectors in an n-dimensional space, where n corresponds to the number of bands (or wavelengths). The similarity between two vectors (spectra) is evaluated by calculating the spectral angle between the two, where a smaller angle indicates a closer match with a particular class of materials. As shown in previous studies [43], SAM can be effective for visualizing pixels with similar spectral behaviors on a false color map and has the potential to distinguish pigment mixtures with a similar hue. Slightly different results can be obtained depending on the choice of the endmembers and the values of the maximum angle thresholds. In this case, the threshold selected for each endmember was 0.100 radians. While preliminary tests were also performed with higher threshold values, the end results of the classification have not significantly changed.

In order to obtain reliable maps, the selection of the endmembers was based on the results obtained from the combined spectroscopic analysis, as discussed in the previous sections. A total of ten endmembers were selected—seven endmembers corresponding to the pigmented surfaces (red pigment, pink pigment, yellow pigment, purple pigment, green pigment, and black pigment) and to the plaster support, plus three additional endmembers corresponding to the experimental conditions (cardboard background, reflectance target, and undesired shadows). Based on FCIR images, the endmembers were selected using the Region of Interest (ROI) tool, which enabled the obtainment of an average value for the selected pixels (see Figure S8). The classification was performed across all 288 bands using a consistent threshold angle, as the characteristic spectral features of the endmembers spanned the entire range of available wavelengths. Since each endmember contained spectral features ascribed to calcite, maintaining the same angle value allowed for the differentiation of specific features unique to each spectral endmember. Figure 9 shows the SAM classification maps for all selected endmembers. As can be observed, the classification maps obtained gave the best results for the green pigments, as well as for the pink and black pigments, and for some of the red areas. Also, SAM accurately classified the surface depositions—such in the case of samples S2 and S7. However, for some of the samples, the algorithm produced mixed results, as the mapping distribution did not align with the spectroscopic data obtained (sample S8). Some limitations were also observed in differentiating the red ochre areas from the yellow ochre ones.

With the aim of further refining the mapping and distribution of the endmembers, Linear Spectral Unmixing (LSU) was also applied. Compared to SAM, LSU can offer better results, especially when used on mixtures, due to the fact that the spectral signal of a pixel is not given by a single component but by a combined number of components [92]. Taking into consideration the fact that IR radiation is able to penetrate opaque layers, in most of the cases, the spectra are a combination of the signals reflected from several materials. LSU is able to highlight the abundance maps of the pixels, which are more likely to belong to a certain class. For this classification, it was applied a unit-sum constraint (or a weight factor). Using the default value, the results consisted in fractions of pixels according to the input endmembers, which took values ranging from 0 to 1. As in the case of SAM, the same

ROI collection was used as input for the endmembers and calculations were made for all 288 bands in the 954–2514 nm region.

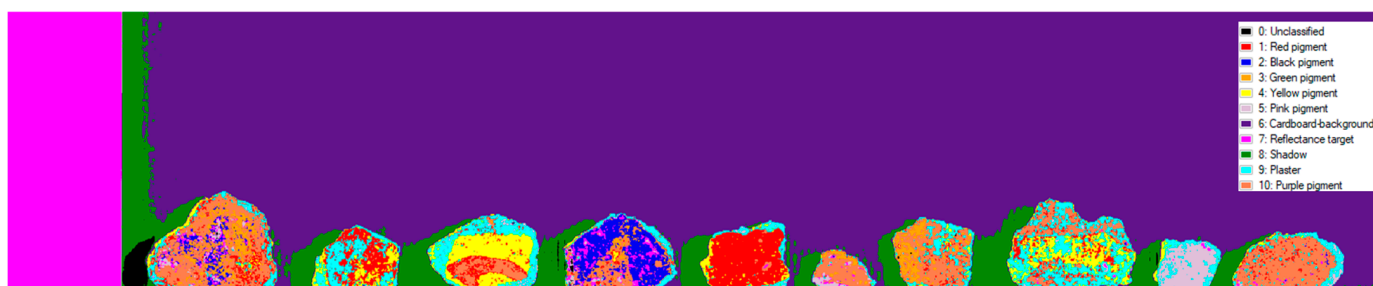


Figure 9. SAM classification maps obtained on the investigated wall painting fragments.

For each category, the algorithm generated a specific grayscale image (abundance map), where lighter tones indicate higher probabilities (better fitting with values close to 1), while darker tones correspond to lower probabilities (values close to 0). As shown in Figure 10a, the abundance map for the red pigment (endmember) yielded better results compared to SAM and perfectly matched the actual/visual distribution of the red ochre pigment. Furthermore, the distribution map validated the hypothesis drawn from XRF analysis, indicating that the same red ochre pigment was used for the top red-pigmented layers (samples S2, S5 and S8) and the red preparation layer (best observed via the lacuna in samples S4). As in the case of SAM classifications, the presence of adherent deposits on the painted surface (best seen in the case of sample S2) and/or the presence of (trace) superimposed pigmented layers were clearly differentiated, with refined results obtained via LSU.

The abundance map obtained for the black pigment (Figure 10b) provided additional insights into the use and distribution of carbon black pigments across the investigated wall painting fragments. Based on the obtained distribution maps of the black pigment endmember, we can infer that a carbon-based black pigment admixed with some earth-based pigment(s) was also used in the case of sample S1 and S10 to obtain the desired dark brown hues. More so, LSU results confirmed the presence of a bone black pigment rich in hydroxyapatite (on top of the red background paint layer) in sample S8, as inferred by FTIR analysis. Interesting results and additional insights were also obtained in the case of the purple pigment endmember. As shown in Figure 10c, bright pixels—indicating higher abundance or fractional covers—were observed not only on the purple-gray paint layer in sample S3 (as expected), but also in sample S1. In this latter case, these bright pixels were distributed across several painted areas, particularly in the outer regions where the superficial paint layers are significantly more degraded. The resulting distribution suggests a certain similarity between these two painted areas that could be due to the use of a similar pigment mixture and/or to the use of a similar type of application. Based on microscopic observations (see Figure 1d), and combined analytical data, we were able to infer the presence of a dark-blue undercoat in sample S1, likely composed of a mixture of carbon black, ochre, and possibly some type of organic component. The LSU classification map obtained using the reference green earth pigment (Figure 10d) as endmember gave unsatisfactory results, with better classifications being registered via SAM.

Because the accuracy of endmember selection is crucial, errors in classification are highly plausible, especially when the spectral variability is not significant, as in this case where similar mineral-based pigments have been used (alone or admixed). Although the resulting classes were displayed with relatively high accuracy in both classifications, some pixels remained unclassified. In both SAM and LSU, part of the shadow cast by the reflectance panel was unclassified because no pixels from that specific area were included during the endmember selection process. This is noticeable in the root mean square (RMS) error image corresponding to the LSU (see Figure S9).

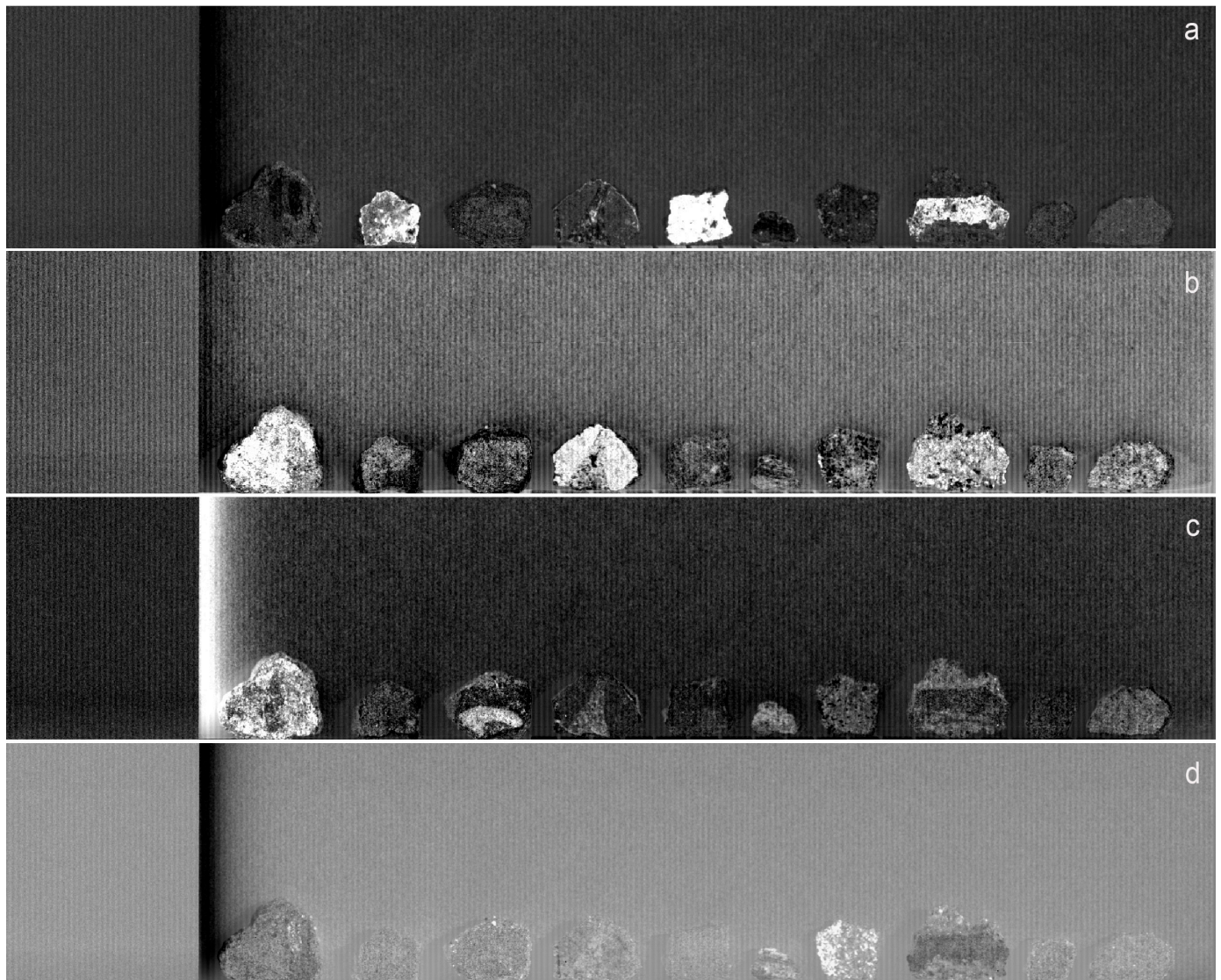


Figure 10. LSU abundance maps obtained on the investigated wall painting fragments: red pigment (a), black pigment (b), purple pigment (c), and green pigment (d). Brighter pixels indicate greater abundance.

In order to increase the discrimination capability of the employed pigmenting materials via HSI, the spectral signatures registered in the SWIR region were also analyzed. The SWIR reflectance spectra (extracted from specific points of interest of the painted surfaces) show some overall similarity in the 1800–2500 nm spectral region, mainly due to the presence of carbonates and clay minerals. As outlined in Figure 11a, the absorptions centered at 2350 nm and at 2500 nm are characteristic of the CO_3^{2-} ion in calcite. Additional carbonate vibrational bands can also occur around 2120 to 2160 nm, 1970 to 2000 nm, and 1850 to 1870 nm [93], with the purity level and composition of the carbonate mineral affecting the positions of these peaks. For samples where the pictorial layers appear thin and degraded (such as in the case of sample S7 for example), the SWIR reflectance spectra registered within these areas are dominated by the spectral contributions coming from the plaster substrate. For such situations the contributions from the clay minerals are more intense—the strong bands around 1400 nm (OH stretch overtones) and 2200 nm (Al–OH bend plus OH stretch combinations)—can be directly linked with the presence of kaolinite [94]. The 1900 nm band, associated with water, is common in several types of minerals, including kaolinite [95].

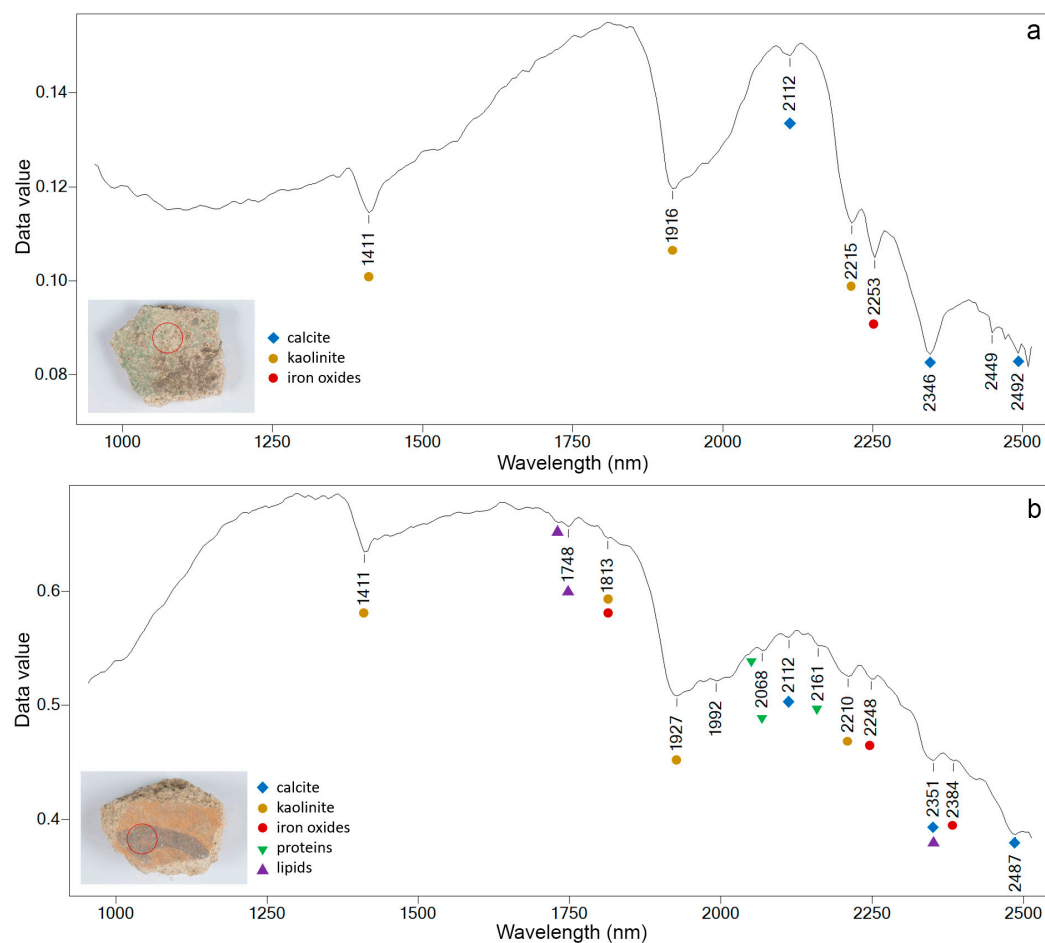


Figure 11. SWIR reflectance spectrum registered on the green paint layer on sample S7 (a) and on the purple paint layer on sample S3 (b).

Based on the capability of near-infrared and short-wave infrared (VNIR-SWIR) spectroscopy to detect the overtones and combination bands of C-H, O-H, N-H, and S-H molecules, the hypothesis regarding the possible use of organic binders, initially inferred through FTIR, was further explored. As shown in previous studies [42,44], organic materials display characteristic spectral features above 1000 nm, having little interference with iron oxide minerals, such as red and yellow ochres for example. Proteins are typically characterized by spectral features at 2042–2063 and 2173–2177 nm, while lipids show characteristic bands around 1700–1760, 2300 and 2350 nm [44,96]. The application of a *secco* technique over the *fresco* background was explored in the case of sample S3, on the decorative purple paint layer. A closer examination of the SWIR reflectance spectra registered in this case (Figure 11b) shows weak but characteristic features, which can be linked with both proteins (peaks at 2041, 2068, and 2161 nm) and potential lipids (1742, 1748, and 2335 nm), suggesting the use of animal glue. Similar features can also be seen in the SWIR spectral profile registered on the faded decorative band (observed starting with the 1600 nm band) on sample S6 (Figure S10), suggesting that this decorative paint layer was applied *a secco*.

4. Discussion and Concluding Remarks

The analyses performed in this study add new data to the current knowledge on the materials and painting techniques used for wall painting decorations in the Roman province of Dacia and make a significant contribution to the archeological research at the Ulpia Traiana Sarmizegetusa site. The employed minimally invasive multi-method approach adopted allowed us to obtain a rich set of data while at the same time preserving the integrity of these precious wall painting fragments. The combined use of non-invasive (XRF)

and micro-invasive spectroscopic techniques (LIBS, ATR-FTIR) and SWIR hyperspectral imaging enabled not only the identification and characterization of the pictorial materials that were used but also the mapping of their distributions. Analytical challenges were encountered for situations where complex inorganic and organic mixtures were used, and for degraded pictorial surfaces where only traces of the original polychromy were still preserved. Additional studies and the use of more refined techniques are needed to further corroborate the hypothesis on the use of organic dyes and determine (with a greater level of confidence) the type of organic materials used [97–99].

Our research studies carried out on Roman wall painting fragments coming from various Roman archeological sites located in Romania [28,29] revealed a rich color palette that included common earth pigments (*colores austeri*), but also, in some particular situations, expensive pigments (*colores floridi*) as well [52]. In the case of this newly analyzed group of wall painting fragments, a very common Roman color palette was found, especially on the large colored areas: red ochre (hematite), yellow ochre (goethite), green earth (celadonite), and carbon-based blacks (soot and bone black). On the upper paint layers of some of the wall painting fragments investigated, some more expensive pigments, such as lead-based pigments and potentially indigo, were also identified, typically admixed with other pigments. The presence of Egyptian blue was also inferred based on indirect evidence.

Although the visible observed palette was not particularly wide in terms of basic colors, the registered data revealed that the painters skillfully expanded the chromatic range by mixing, diluting (with water or lime white), concentrating, or altering the grain size of the basic pigments (such in the case of the red ochre). Compared to previous findings within the region [28,29], in this group of wall painting fragments, a higher number of pigment mixtures could be highlighted. Some of the green hues were obtained by mixing green earth with grains of Egyptian blue and yellow ochre; purple hues were probably obtained by mixing indigo, carbon black, and a lead-based pigment; the light-blue hues were based on a mixture of lazurite, calcite, and possibly small amounts of indigo; the dark-brown hues were obtained by mixing iron-rich ochres with carbon black; and the pink hues were produced by the common and simple mixture of red ochre with lime white. These findings reflect the high technical know-how of the craftsmen in obtaining the desired chromatic effects by mixing and layering pigments. The addition of carbon black to the relatively transparent earth-based pigments acts as an opacifier [50]. Interestingly, mixtures like those identified in the black-painted layer were mentioned by Pliny as being used for specific painting purposes, such as undercoat layers for cinnabar and red lead pigments [100]. Given the small size of the preserved wall painting fragments investigated, it is plausible that such layers once existed on the original wall painting decoration.

All of the identified pigments are consistent with those observed throughout the Roman Empire and correspond with the palette described by historical sources. The use of indigo, a pigment listed by Pliny among the more expensive ones [52], was documented for the first time in the region as a potential finding (with further studies needed to confirm this hypothesis). Along with red lead [28] and cinnabar [22], these are the most precious and expensive pigments discovered so far in the Roman province of Dacia.

Egyptian blue, an ancient synthetic pigment widely used by the Romans, was found for the first time within wall painting fragments excavated at the Ulpia Traiana Sarmizegetusa archeological site. Until now, only two occurrences of Egyptian blue have been documented in the region, both found in mural painting fragments from richly decorated houses of the high Roman aristocracy at the Roman settlement of Apulum II [22] and Rapoltu Mare [30]. The occurrence of Egyptian blue on green paint layers infers the idea that small quantities were added (along with goethite) to the green earths to alter the color tone, a practice documented in several other studies [65,69,70]. While pure Egyptian blue paint layers may have been originally applied, the preserved polychromy highlighted in this case only contains traces of this blue pigment. Based on macroscopic observations and registered data, it is likely that some Egyptian blue decorative details were applied over an optical blue underlayer (obtained by mixing carbon black and calcite), which is in agreement with historical sources.

As expected, most of the preserved colored layers were found to be based on iron-rich earth pigments and minerals. Both red (hematite) and yellow (goethite) ochre have been previously documented within the region [25,28–30]. Green earths based on celadonite have also been previously found [28–30]. As already discussed in a previous study [29], the ochres used for the various wall painting fragments discovered across different archaeological sites in Dacia may have the same geological source. According to the registered XRF data, the chemical fingerprints registered for these pigments are very similar, including elements such as Ti, Mn, Cu, As, Pb, Cr, and Zn. As shown in other studies, heavy metals, such as arsenic and lead, have proven to be useful indicators when studying ochre provenance [57,101]. Furthermore, recent studies have shown that arsenic can be used as a key heavy metal tracer element for the discrimination between original red ochre and a red-colored transformed yellow ochre [102]. However, the lack of available mineral fingerprint databases makes it impossible at the moment to formulate any solid hypotheses regarding the provenance of the ochres used. The potential influence of adulterations and the addition of other components to ochre pigments, widely used in the Roman world, introduces further challenges. Moreover, in this case, given the fact that the XRF elemental analysis was performed without sampling, probing the whole stratigraphy, matrix effects need to be taken into account. Not least, in some of the investigated areas, the levels of both arsenic and lead seem higher than typically expected for natural occurrence in ochre pigments. This suggests the possibility that arsenic- and lead-based pigments could have been intentionally added to the ochre pigments to modify their color, a practice documented in the literature [61].

Two carbon-based black pigments could be identified in this study—soot (admixed with an ochre-based pigment), and bone black—both pigments being mentioned by Pliny. Within the province of Dacia, amorphous carbon-based black pigments (soot/coal) have been previously found at Rapoltu Mare [30], while in the case of the murals discovered at the Roman baths from Alburnus Maior, the black pigment employed was found to be a manganese-rich black ochre [29]. Regarding white pigments, the group of wall painting fragments investigated in this study does not show any white decorations or clear white background areas. However, for the lighter hues, such as pink, the use of calcite (lime white) admixed with red ochre can be inferred. The use of lead white, as an express whitening agent employed to obtain the desired hue [50], may also have been used based on the registered data. The use of strontianite, a rare white carbonate mineral, identified in previous Roman-age murals coming from the same archaeological site [28], can be ruled out in this case.

The results obtained through the combined multi-analytic approach suggest that the original wall decorations of some of the investigated fragments had a more complex polychromy compared to what we see today, likely featuring brighter hues. Thus, the use of a wider range of pigments at the time the wall paintings were created cannot be excluded. While surface abrasion and overall (natural) degradation of the wall paintings have caused fading of the pigments and the irreversible loss of the original polychromy, hyperspectral imaging was able to retrieve some faded paint layers in certain cases, helping to recover lost decorative details. This suggests a promising application of HSI for rapid, non-invasive mural information enhancement, including the possibility of virtual restoration when combined with deep learning methods [103].

A red preparation layer (*sinopia*) based on red ochre was found in the case of several wall paintings fragments, with the layer being applied directly on the *arriccio*. The presence of this underlayer (documented for the first time in the region), which serves as the preparatory drawing, clearly suggests that the artist's graphic work was highly complex, requiring careful planning of the scale and position of the main figures/decorative elements in relation to the wall space [3]. More so, the use of expensive pigments, typically reserved for painted artworks of particular value and for selected figurative motifs (to emphasize the symbolic significance of a composition), is another clear indicator that the original wall paintings had an elaborate schema. The presence of these preliminary red sketches, along with the use of expensive colors and complex mixtures, reflect the craftsmen's

high technical know-how as well as the patron's wealth and social status [1]. It is well documented that only the elite would have been able to afford elaborate wall paintings in the most expensive colors, with the homeowner responsible for supplying these rare and precious pigments. Most probably, the investigated wall painting fragments belong to the more finely decorated rooms of the *Domus Procuratoris*, with colored grounds and refined techniques being reserved for such areas [3].

In terms of painting technique, the presence of an organic binder may have been used for finishing the superimposed paint layers, with weak but characteristic bands for proteinaceous compounds being observed in the FTIR and SWIR reflectance spectra registered in these areas. The use of the *a secco* technique, which involves mixing organic binders with pigments and applying them to dry plaster, has been documented in several other studies focused on Pompeian murals. These studies have shown the presence of amino acids, sugars, and fatty acids associated with the use of flours, gums, and oils [104], as well as the presence of proteinaceous material, most likely egg [69]. Traces of a protein binder have also been found in the preserved painted plasters discovered at the Roman baths from Alburnus Maior [29], while in the case of the wall painting fragments from Rapoltu Mare, beeswax was identified [30]. However, as shown in other studies, the presence of beeswax is most probably associated with past conservation treatments [105]. Our first study carried out on wall painting fragments coming from Ulpia Traiana Sarmizegetusa highlighted the use of a *fresco-secco* technique (with lime as a binder), with no organic binders being identified [28]. Yet, in a following study, investigations carried out on new fragments with superimposed paint layers revealed the application of *a secco* technique over the *fresco* background [29]. The current findings are, therefore, in agreement with our previous studies and underscore the existence of well-established practices in the region.

Overall, we believe that this study adds an important contribution to the existing body of data on Roman wall painting decorations in Dacia, particularly regarding the identification of expensive pigments (including the possible use of organic dyes), complex pigment mixtures, and organic binders. Furthermore, the reported findings not only provide new insights into the painting production methods employed by ancient artists in this region of the Roman Empire but also offer valuable information about Roman daily life, residential decoration, and the ways in which wealth and status were expressed through private building projects.

Supplementary Materials: The following supporting information can be downloaded at: <https://www.mdpi.com/article/10.3390/heritage7090248/s1>, Figure S1: Optical microscopy images that highlight the existence of more complex decorative patterns (with superimposed paint layers, and/or the use of pigment mixtures: light-blue decorative paint layer applied on top of a black underground (sample S4) (a); light-blue decorative paint layers (in various shades) applied on top of an optical blue undercoat (sample S6) (b); complex polychromy, highly degraded, applied on a reddish-brown preparatory layer (sample S1) (c); traces of yellow ochre and other colored inclusions on top of the greyish-green underground (sample S10) (d).; Figure S2: Comparison of XRF spectra corresponding to red areas, evidencing the $K\alpha$ and $K\beta$ lines of As; Figure S3: LIBS stratigraphic distribution on sample S6 for C, Si, Pb, Al, Fe, Sr, K and Cu; Figure S4: Comparative FTIR spectra of the top grayish paint layer (with black line) and the red paint layer underneath (with red line); Figure S5: FTIR spectrum registered on the dark-brown paint layer on sample S1; Figure S6: FTIR spectrum registered on the green painted areas on sample S4 (with black line) and the second derivative profile (with green line). The second derivative was obtained using the Savitzky–Golay method; Figure S7: FTIR spectrum registered on the intonaco layer on sample S2; Figure S8: Spatial Region of Interest (ROI) selection; Figure S9: The root-mean-square (RMS) error image corresponding to the LSU classification; Figure S10: SWIR reflectance spectrum registered on the faded decorative band layer (observed starting with the 1600 nm band) on sample S6; Table S1: Results of the LIBS stratigraphic analysis.

Author Contributions: Conceptualization, I.M.C. and O.T.; methodology, I.M.C.; investigation, I.M.C., L.G., L.R. and M.D.; data curation, I.M.C., L.G., L.R. and M.D.; writing—original draft preparation, I.M.C., L.G., O.T., L.R. and M.D.; writing—review and editing, I.M.C., L.G., O.T., L.R.

and M.D.; resources, O.T.; funding acquisition, I.M.C. All authors have read and agreed to the published version of the manuscript.

Funding: This work was supported by a grant from the Ministry of Research, Innovation and Digitization, CCCDI—UEFISCDI, project number PN-III-P2-2.1-PED-2021-3576, within PNCDI III, and through the Core Program within the National Research Development and Innovation Plan 2022-2027, project no. PN 23 05.

Data Availability Statement: The original contributions presented in the study are included in the article/Supplementary Materials, further inquiries can be directed to the corresponding author.

Conflicts of Interest: The authors declare no conflicts of interest.

References

1. Salvadori, M.; Sbrolli, C. Wall paintings through the ages: The roman period—Republic and early Empire. *Archaeol. Anthr. Sci.* **2021**, *13*, 187. [\[CrossRef\]](#)
2. Pappalardo, U. *The Splendor of Roman Wall Painting*; J. Paul Getty Museum: Los Angeles, CA, USA, 2009.
3. Ling, R. *Roman Painting*; Cambridge University Press: New York, NY, USA, 1991.
4. Davy, H. LXIII. Some Experiments and Observations on the Colours Used in Painting by the Ancients. *Philos. Mag.* **1815**, *45*, 349–359. [\[CrossRef\]](#)
5. Chaptal, J.A. Sur Quelques Couleurs Trouvées à Pompeïa. *Ann. Chim.* **1809**, *70*, 22–31.
6. Cuní, J. What Do We Know of Roman Wall Painting Technique? Potential Confounding Factors in Ancient Paint Media Analysis. *Herit. Sci.* **2016**, *4*, 44. [\[CrossRef\]](#)
7. Zhu, Z.; Yao, X.; Qin, Y.; Lu, Z.; Ma, Q.; Zhao, X.; Liu, L. Visualization and Mapping of Literature on the Scientific Analysis of Wall Paintings: A Bibliometric Analysis from 2011 to 2021. *Herit. Sci.* **2022**, *10*, 105. [\[CrossRef\]](#)
8. Mazzocchin, G.A.; Rudello, D.; Murgia, E. Analysis of Roman Wall Paintings Found in Verona. *Ann. Chim.* **2007**, *97*, 807–822. [\[CrossRef\]](#)
9. Garofano, I.; Perez-Rodriguez, J.L.; Robador, M.D.; Duran, A. An Innovative Combination of Non-Invasive UV-Visible-FORS, XRD and XRF Techniques to Study Roman Wall Paintings from Seville, Spain. *J. Cult. Herit.* **2016**, *22*, 1028–1039. [\[CrossRef\]](#)
10. Dooryhée, E.; Anne, M.; Bardiès, I.; Hodeau, J.-L.; Martinetto, P.; Rondot, S.; Salomon, J.; Vaughan, G.B.M.; Walter, P. Non-Destructive Synchrotron X-Ray Diffraction Mapping of a Roman Painting. *Appl. Phys. A Mater. Sci. Process.* **2005**, *81*, 663–667. [\[CrossRef\]](#)
11. Béarat, H. Chemical and Mineralogical Analyses of Gallo-Roman Wall Painting from Dietikon, Switzerland. *Archaeometry* **1996**, *38*, 81–95. [\[CrossRef\]](#)
12. Edwards, H.G.M.; Middleton, P.S.; Hargreaves, M.D. Romano-British Wall Paintings: Raman Spectroscopic Analysis of Fragments from Two Urban Sites of Early Military Colonisation. *Spectrochim. Acta Part A Mol. Biomol. Spectrosc.* **2009**, *73*, 553–560. [\[CrossRef\]](#)
13. Apostolaki, C.; Perdikatsis, V.; Repuskou, E.; Brecoulaki, H.; Lepinski, S. Analysis of Roman Wall Paintings from Ancient Corinth/Greece. In Proceedings of the 2nd International Conference on: Advances in Mineral Resources, Hania, Greece, 25–27 September 2006; pp. 729–734.
14. Radpour, R.; Fischer, C.; Kakoulli, I. New Insight into Hellenistic and Roman Cypriot Wall Paintings: An Exploration of Artists' Materials, Production Technology, and Technical Style. *Arts* **2019**, *8*, 74. [\[CrossRef\]](#)
15. Smith, D.C.; Barbet, A. A Preliminary Raman Microscopic Exploration of Pigments in Wall Paintings in the Roman Tomb Discovered at Kertch, Ukraine, in 1891. *J. Raman Spectrosc.* **1999**, *30*, 319–324. [\[CrossRef\]](#)
16. Gutman, M.; Zanier, K.; Lux, J.; Kramar, S. Pigment Analysis of Roman Wall Paintings from Two Villae Rusticae in Slovenia. *Mediterr. Archaeol. Archaeom.* **2016**, *16*, 193. [\[CrossRef\]](#)
17. Babeş-Bolyai, U.; Olteanu, B.-C. Stadiul cercetărilor pluridisciplinare asupra fragmentelor de tencuiă pictată din Dacia. *Cercet. Arheol.* **2022**, *29*, 149–154. [\[CrossRef\]](#)
18. Mora, P.; Mora, L.; Philippot, P. *Conservation of Wall Paintings*; Butterworths: London, UK, 1984.
19. Ciobanu, R. *Pictura Murală Romană (La Peinture Murale Romaine)*; Editura Grinta: Alba Iulia, Romania, 2011.
20. Ciobanu, R. Le décor monumental en Dacie romaine. Ph.D. Thesis, Université Paris 1 Panthéon-Sorbonne, Paris, France, 1995.
21. Rusu-Bolindeţ, V.; Ilea, C.; Volkens, T. Alba Iulia, jud. Alba [Apulum]. In *Cronica Cercetărilor Arheologice din România. Campania 2000*; Angelescu, M.V., Borş, C., Oberlander Târnoveanu, I., Eds.; CiMEC: Bucureşti, Romania, 2001; pp. 25–26.
22. Ciobanu, R. The Paintings Hall with Hypocausts from Apulum II. *Apulum* **2005**, *42*, 123–136.
23. Tentea, O.; Olteanu, B. Fresca unei locuințe din Secolul II p.Chr. de la Sarmizegetusa. *Cercet. Arheol.* **2018**, *25*, 91–104. [\[CrossRef\]](#)
24. Barbu, M.G.; Bărbat, A.I.; Băeştean, G.; Bălos, G.; Gonciar, A.; Brown, A. Raport preliminar privind cercetările arheologice de la Rapoltu Mare-La Vie, Campaniile 2013–2015. *Banatica* **2016**, *26*, 273–321.
25. Boros, D.; Duca, V. Tencuiala pictată din amfiteatrul de la Porolissum (Considerații Tehnice). *Acta Musei Porolissensis* **2008**, *30*, 113–121.
26. Tentea, O. *Bath and Bathing at Alburnus Maior*; Mega Publishing House: Cluj-Napoca, Romania, 2015; ISBN 978-606-543-429-5.
27. Boros, D. Studiul tehnic al unor fragmente arheologice de tencuiă pictată. *Acta Musei Porolissensis* **2003**, *25*, 719–723.

28. Corcea, I.M.; Ghervase, L.; Țentea, O.; Pârău, A.C.; Radvan, R. First Analytical Study on Second-Century Wall Paintings from Ulpia Traiana Sarmizegetusa: Insights on the Materials and Painting Technique. *Int. J. Arch. Herit.* **2020**, *14*, 751–761. [[CrossRef](#)]
29. Corcea, I.M.; Ratoiu, L.; Ghervase, L.; Țentea, O.; Dinu, M. Investigation of Ancient Wall Painting Fragments Discovered in the Roman Baths from Alburnus Maior by Complementary Non-Destructive Techniques. *Appl. Sci.* **2021**, *11*, 10049. [[CrossRef](#)]
30. Ion, R.-M.; Barbu, M.G.; Gonciar, A.; Vasilievici, G.; Gheboianu, A.I.; Slamnoiu-Teodorescu, S.; David, M.E.; Iancu, L.; Grigorescu, R.M. A Multi-Analytical Investigation of Roman Frescoes from Rapoltu Mare (Romania). *Coatings* **2022**, *12*, 530. [[CrossRef](#)]
31. Alicu, D. 80 de Ani de Cercetări Arheologice La Ulpia Traiana Sarmizegetusa. *Sargetia* **2003**, *31*, 253–258.
32. Piso, I. Colonia Ulpia Traiana Augusta Dacica Sarmizegetusa. Brève Présentation et État de Recherché. *Transylv. Rev.* **2001**, *10*, 16–37.
33. Piso, I. *An der Nordgrenze des Römischen Reiches. Ausgewählte Studien (1972–2003)*; Franz Steiner Verlag: Stuttgart, Germany, 2005; ISBN 978-3-515-08729-2.
34. Țentea, O.; Olteanu, B.C. Decorating Overlapping Buildings: A Domus and Palmyrene Temple at Colonia Dacica Sarmizegetusa. *Theor. Rom. Archaeol. J.* **2020**, *3*, 6. [[CrossRef](#)]
35. Piso, I.; Țentea, O. Un Nouveau Temple Palmyrénien à Sarmizegetusa. *Dacia—Rev. d'Archéologie d'Hist. Ancienne* **2011**, *55*, 111–122.
36. Caneve, L.; Diamanti, A.; Grimaldi, F.; Palleschi, G.; Spizzichino, V.; Valentini, F. Analysis of Fresco by Laser Induced Breakdown Spectroscopy. *Spectrochim. Acta—Part B At. Spectrosc.* **2010**, *65*, 702–706. [[CrossRef](#)]
37. Dinu, M.; Corcea, I.M.; Ghervase, L.; Stancu, M.C.; Mohanu, I.; Cristea, N. Optoelectronic Investigation of the Mural Paintings from Drăguțești Wooden Church, Argeș County, Romania. *J. Optoelectron. Adv. Mater.* **2020**, *2020*, 303–309.
38. Paladini, A.; Toschi, F.; Colosi, F.; Rubino, G.; Santoro, P. Stratigraphic Investigation of Wall Painting Fragments from Roman Villas of the Sabina Area. *Appl. Phys. A Mater. Sci. Process.* **2015**, *118*, 131–138. [[CrossRef](#)]
39. Lazic, V.; Fantoni, R.; Falzone, S.; Gioia, C.; Loreti, E.M. Stratigraphic Characterization of Ancient Roman Frescos by Laser Induced Breakdown Spectroscopy and Importance of a Proper Choice of the Normalizing Lines. *Spectrochim. Acta—Part B At. Spectrosc.* **2020**, *168*, 105853. [[CrossRef](#)]
40. Fermo, P.; Piazzalunga, A.; Vos, M.; Andreoli, M. A Multi-Analytical Approach for the Study of the Pigments Used in the Wall Paintings from a Building Complex on the Caelian Hill (Rome). *Appl. Phys. A* **2013**, *113*, 1109–1119. [[CrossRef](#)]
41. Piqué, F.; Verri, G. (Eds.) *Organic Materials in Wall Paintings (Project Report)*; The Getty Conservation Institute: Los Angeles, CA, USA, 2015; ISBN 978-1-937433.
42. Cloutis, E.; MacKay, A.; Norman, L.; Goltz, D. Identification of Historic Artists' Pigments Using Spectral Reflectance and X-Ray Diffraction Properties I. Iron Oxide and Oxy-Hydroxide-Rich Pigments. *J. Near Infrared Spectrosc.* **2016**, *24*, 27–45. [[CrossRef](#)]
43. Cucci, C.; Picollo, M.; Chiarantini, L.; Uda, G.; Fiori, L.; De Nigris, B.; Osanna, M. Remote-Sensing Hyperspectral Imaging for Applications in Archaeological Areas: Non-Invasive Investigations on Wall Paintings and on Mural Inscriptions in the Pompeii Site. *Microchem. J.* **2020**, *158*, 105082. [[CrossRef](#)]
44. Horn, K.R. Time Takes Its Toll: Detection of Organic Binder Media in Ochre Paints with Visible Near-Infrared and Short-Wave Infrared Reflectance Spectroscopy. *J. Archaeol. Sci. Rep.* **2018**, *21*, 10–20. [[CrossRef](#)]
45. Daicovicu, H.; Alicu, D. *Colonia Ulpia Traiana Augusta Dacica Sarmizegetusa*; Sport-Turism: București, Romania, 1984.
46. Piso, I. *Fasti provinciae Daciae. I, Die Senatorischen Amtsträger*; R. Habelt: Bonn, Germany, 1993.
47. Piso, I. Inschriften von Prokuratoren aus Sarmizegetusa (II). *Z. Papyrol. Epigr.* **1998**, *120*, 253–271.
48. Maguregui, M.; Castro, K.; Morillas, H.; Trebolazabala, J.; Knuutinen, U.; Wiesinger, R.; Schreiner, M.; Madariaga, J.M. Multi-Analytical Approach to Explain the Darkening Process of Hematite Pigment in Paintings from Ancient Pompeii after Accelerated Weathering Experiments. *Anal. Methods* **2014**, *6*, 372–378. [[CrossRef](#)]
49. Finch, A.A.; Allison, N. Coordination of Sr and Mg in Calcite and Aragonite. *Miner. Mag.* **2007**, *71*, 539–552. [[CrossRef](#)]
50. Secco, M.; Rainer, L.; Graves, K.; Heginbotham, A.; Artioli, G.; Piqué, F.; Angelini, I. Ochre-Based Pigments in the Tablinum of the House of the Bicentenary (Herculaneum, Italy) between Decorative Technology and Natural Disasters. *Minerals* **2021**, *11*, 67. [[CrossRef](#)]
51. Siddall, R. Mineral Pigments in Archaeology: Their Analysis and the Range of Available Materials. *Minerals* **2018**, *8*, 201. [[CrossRef](#)]
52. Siddall, R. Not a Day without a Line Drawn: Pigments and Painting Techniques of Roman Artists. *Infocus Mag.* **2006**, *2*, 18–31. [[CrossRef](#)]
53. Corcea, I.M.; Ghervase, L.; Rădvan, R.; Seritan, G. Assessment of Easily Accessible Spectroscopic Techniques Coupled with Multivariate Analysis for the Qualitative Characterization and Differentiation of Earth Pigments of Various Provenance. *Minerals* **2022**, *12*, 755. [[CrossRef](#)]
54. Westlake, P.; Siozos, P.; Philippidis, A.; Apostolaki, C.; Derham, B.; Terlix, A.; Perdikatsis, V.; Jones, R.; Anglos, D. Studying Pigments on Painted Plaster in Minoan, Roman and Early Byzantine Crete. A Multi-Analytical Technique Approach. *Anal. Bioanal. Chem.* **2012**, *402*, 1413–1432. [[CrossRef](#)] [[PubMed](#)]
55. Gil, M.; Carvalho, M.; Seruya, A.; Candeias, A.; Mirão, J.; Queralt, I. Yellow and Red Ochre Pigments from Southern Portugal: Elemental Composition and Characterization by WDXRF and XRD. *Nucl. Instruments Methods Phys. Res. Sect. A Accel. Spectrometers Detect. Assoc. Equip.* **2007**, *580*, 728–731. [[CrossRef](#)]

56. Marcaida, I.; Maguregui, M.; Morillas, H.; Prieto-Taboada, N.; de Vallejuelo, S.F.-O.; Veneranda, M.; Madariaga, J.M.; Martellone, A.; De Nigris, B.; Osanna, M. In Situ Non-Invasive Characterization of the Composition of Pompeian Pigments Preserved in their Original Bowls. *Microchem. J.* **2018**, *139*, 458–466. [[CrossRef](#)]
57. Popelka-Filcoff, R.S.; Robertson, J.D.; Glascock, M.D.; Descantes, C. Trace Element Characterization of Ochre from Geological Sources. *J. Radioanal. Nucl. Chem.* **2007**, *272*, 17–27. [[CrossRef](#)]
58. Dai, M.; Zhou, Y.; Xiao, Q.; Lv, J.; Huang, L.; Xie, X.; Hu, Y.; Tong, X.; Chun, T. Arsenic Removal and Iron Recovery from Arsenic-Bearing Iron Ores by Calcification-Magnetic Roasting and Magnetic Separation Process. *Materials* **2023**, *16*, 6884. [[CrossRef](#)]
59. Hizal, J.; Apak, R. Modeling of Copper(II) and Lead(II) Adsorption on Kaolinite-Based Clay Minerals Individually and in the Presence of Humic Acid. *J. Colloid Interface Sci.* **2006**, *295*, 1–13. [[CrossRef](#)]
60. Dong, D.-M.; Zhao, X.-M.; Hua, X.-Y.; Zhang, J.-J.; Wu, S.-M. Lead and Cadmium Adsorption onto Iron Oxides and Manganese Oxides in the Natural Surface Coatings Collected on Natural Substances in the Songhua River of China. *Chem. Res. Chin. Univ.* **2007**, *23*, 659–664. [[CrossRef](#)]
61. Béarat, H. Quelle Est La Gamme Exacte Des Pigments Romains? Confrontation Des Resultats d’analyse et Des Textes de Vitruve et de Pline. In *Roman Wall Painting: Materials, Techniques, Analysis and Conservation. Proceedings of the International Workshop, Fribourg, Switzerland, 7–9 March 1996*; Institute of Mineralogy and Petrography: Fribourg, Switzerland, 1997; pp. 11–34.
62. Eastaugh, N.; Walsh, V.; Chaplin, T.; Siddall, R. (Eds.) *Pigment Compendium: A Dictionary and Optical Microscopy of Historical Pigments*, 1st ed.; Routledge: London, UK, 2008.
63. de Oliveira, L.F.; Edwards, H.G.M.; Frost, R.L.; Klopogge, J.T.; Middleton, P.S. Caput Mortuum: Spectroscopic and Structural Studies of an Ancient Pigment. *Analyst* **2002**, *127*, 536–541. [[CrossRef](#)]
64. Fuchs, M.; Bearat, H. Analyses Physico-Chimiques et Peintures Murales Romaines à Avenches, Bösing, Dietikon et Vallon. In *Roman Wall Painting: Materials, Techniques, Analyses and Conservation. Proceedings of the International Workshop, Fribourg, Switzerland, 7–9 March 1996*; Institute of Mineralogy and Petrography: Fribourg, Switzerland, 1997; pp. 181–191.
65. Jorge-Villar, S.E.; Edwards, H.G.M. Green and Blue Pigments in Roman Wall Paintings: A Challenge for Raman Spectroscopy. *J. Raman Spectrosc.* **2021**, *52*, 2190–2203. [[CrossRef](#)]
66. Clarke, M.; Fredrickx, P.; Colombini, M.P.; Andreotti, A.; Wouters, J.; Van Bommel, M.; Eastaugh, N.; Walsh, V.; Chaplin, T.; Siddall, R. Pompei purpurissum pigment problems. In *Proceedings of the Art’05—8th International Conference on Non-Destructive Investigation, Microanalysis and Diagnostics for the Conservation and Environmental Monitoring of Cultural and Environmental Heritage, Lecce, Italy, 15–19 May 2005*.
67. Aceto, M. Pigments—The Palette of Organic Colourants in Wall Paintings. *Archaeol. Anthr. Sci.* **2021**, *13*, 159. [[CrossRef](#)]
68. Mazzocchin, G.; Agnoli, F.; Colpo, I. Analysis of pigments from Roman wall paintings found in Vicenza. *Talanta* **2003**, *61*, 565–572. [[CrossRef](#)] [[PubMed](#)]
69. Pérez-Diez, S.; Caruso, F.; Nardini, E.F.; Stollenwerk, M.; Maguregui, M. Secco Painting Technique Revealed in Non-Restored Pompeian Murals by Analytical and Imaging Techniques. *Microchem. J.* **2023**, *194*, 109365. [[CrossRef](#)]
70. Linn, R. Layered Pigments and Painting Technology of the Roman Wall Paintings of Caesarea Maritima. *J. Archaeol. Sci. Rep.* **2017**, *11*, 774–781. [[CrossRef](#)]
71. Fort, R.; Varas-Muriel, M.; Zoghalmi, K.; Ergenç, D.; Zaddem, A. Analytical Characterisation of 1st- and 2nd-Century Roman Mortars at the Utica Archaeological Site (Tunisia): Construction Phases and Provenance of the Raw Materials. *J. Archaeol. Sci. Rep.* **2024**, *54*, 104404. [[CrossRef](#)]
72. Namowicz, C.; Trentelman, K.; McGlinchey, C. XRF of Cultural Heritage Materials: Round-Robin IV—Paint on canvas. *Powder Diffr.* **2009**, *24*, 124–129. [[CrossRef](#)]
73. Pye, E. Wall Painting in the Roman Empire: Colour, Design and Technology. *Archaeol. Int.* **2000**, *4*, 24–27. [[CrossRef](#)]
74. Helwig, K. The characterisation of iron earth pigments using infrared spectroscopy. In *Proceedings of the Second Infrared and Raman User’s Group (IRUG 2) Conference, London, UK, 12–13 September 1995*; pp. 83–92.
75. Serna, C.J.; Rendon, J.L.; Iglesias, J.E. Infrared Surface Modes in Corundum-Type Microcrystalline Oxides. *Spectrochim. Acta Part A Mol. Spectrosc.* **1982**, *38*, 797–802. [[CrossRef](#)]
76. Mañosa, J.; la Rosa, J.C.-D.; Silvello, A.; Maldonado-Alameda, A.; Chimenos, J.M. Kaolinite Structural Modifications Induced by Mechanical Activation. *Appl. Clay Sci.* **2023**, *238*, 106918. [[CrossRef](#)]
77. Shahverdi-Shahraki, K.; Ghosh, T.; Mahajan, K.; Aji, A.; Carreau, P.J. Effect of Dry Grinding on Chemically Modified Kaolin. *Appl. Clay Sci.* **2015**, *105–106*, 100–106. [[CrossRef](#)]
78. Nuevo, M.; Sandford, S.A.; Flynn, G.J.; Wirick, S. Mid-Infrared Study of Stones from the Sutter’S Mill Meteorite. *Meteorit. Planet. Sci.* **2014**, *49*, 2017–2026. [[CrossRef](#)]
79. Salama, W.; El Aref, M.; Gaupp, R. Spectroscopic Characterization of Iron Ores Formed in Different Geological Environments Using FTIR, XPS, Mössbauer Spectroscopy and Thermoanalyses. *Spectrochim. Acta Part A Mol. Biomol. Spectrosc.* **2015**, *136*, 1816–1826. [[CrossRef](#)] [[PubMed](#)]
80. Buckley, H.A.; Bevan, J.C.; Brown, K.M.; Johnson, L.R.; Farmer, V.C. Glauconite and Celadonite: Two Separate Mineral Species. *Miner. Mag.* **1978**, *42*, 373–382. [[CrossRef](#)]
81. Garofano, I.; Duran, A.; Perez-Rodriguez, J.L.; Robador, M.D. Natural Earth Pigments From Roman and Arabic Wall Paintings Revealed by Spectroscopic Techniques. *Spectrosc. Lett.* **2011**, *44*, 560–565. [[CrossRef](#)]

82. Bikiaris, D.; Danilia, S.; Sotiropoulou, S.; Katsimbiri, O.; Pavlidou, E.; Moutsatsou, A.; Chryssoulakis, Y. Ochre-Differentiation through Micro-Raman and Micro-FTIR Spectroscopies: Application on Wall Paintings at Meteora and Mount Athos, Greece. *Spectrochim. Acta Part A Mol. Biomol. Spectrosc.* **2000**, *56*, 3–18. [[CrossRef](#)] [[PubMed](#)]
83. Roy, A. (Ed.) *Artists' Pigments. In A Handbook of Their History and Characteristics*; National Gallery of Art: Washington, DC, USA, 1993; Volume 2.
84. Cortea, I.M.; Chiroșca, A.; Angheluță, L.M.; Seritan, G. INFRA-ART: An Open Access Spectral Library of Art-related Materials as a Digital Support Tool for Cultural Heritage Science. *J. Comput. Cult. Herit.* **2023**, *16*, 1–11. [[CrossRef](#)]
85. Jorge-Villar, S.E.; Rodríguez Temiño, I.; Edwards, H.G.M.; Jiménez Hernández, A.; Ruiz Cecilia, J.I.; Miralles, I. The Servilia Tomb: An Architecturally and Pictorially Important Roman Building. *Archaeol. Anthr. Sci.* **2018**, *10*, 1207–1223. [[CrossRef](#)]
86. Lluveras-Tenorio, A.; Spepi, A.; Pieraccioni, M.; Legnaioli, S.; Lorenzetti, G.; Palleschi, V.; Vendrell, M.; Colombini, M.P.; Tinè, M.R.; Duce, C.; et al. A Multi-Analytical Characterization of Artists' Carbon-Based Black Pigments. *J. Therm. Anal. Calorim.* **2019**, *138*, 3287–3299. [[CrossRef](#)]
87. Vila, A.; Ferrer, N.; García, J.F. Chemical Composition of Contemporary Black Printing Inks Based on Infrared Spectroscopy: Basic Information for the Characterization and Discrimination of Artistic Prints. *Anal. Chim. Acta* **2007**, *591*, 97–105. [[CrossRef](#)]
88. Casoli, A. Research on the Organic Binders in Archaeological Wall Paintings. *Appl. Sci.* **2021**, *11*, 9179. [[CrossRef](#)]
89. Dariz, P.; Schmid, T. Trace Compounds in Early Medieval Egyptian Blue Carry Information on Provenance, Manufacture, Application, and Ageing. *Sci. Rep.* **2021**, *11*, 11296. [[CrossRef](#)] [[PubMed](#)]
90. Prieto-Taboada, N.; Fdez-Ortiz de Vallejuelo, S.; Santos, A.; Veneranda, M.; Castro, K.; Maguregui, M.; Morillas, H.; Arana, G.; Martellone, A.; de Nigris, B.; et al. Understanding the Degradation of the Blue Colour in the Wall Paintings of Ariadne's House (Pompeii, Italy) by Non-Destructive Techniques. *J. Raman Spectrosc.* **2021**, *52*, 85–94. [[CrossRef](#)]
91. Herens, E. Study of Antique and Modern Paintings by Hyperspectral Imaging. PhD Thesis, Université de Liège, Liège, Belgium, 2022.
92. Bioucas-Dias, J.M.; Plaza, A.; Dobigeon, N.; Parente, M.; Du, Q.; Gader, P.; Chanussot, J. Hyperspectral Unmixing Overview: Geometrical, Statistical, and Sparse Regression-Based Approaches. *IEEE J. Sel. Top. Appl. Earth Obs. Remote Sens.* **2012**, *5*, 354–379. [[CrossRef](#)]
93. Alayet, F.; Mezned, N.; Sebai, A.; Abdeljaouad, S. Continuum Removed Band Depth Analysis for Carbonate Mining Waste Quantification Using X-Ray Diffraction and Hyperspectral Spectroscopy in the North of Tunisia. *J. Appl. Remote Sens.* **2017**, *11*, 16021. [[CrossRef](#)]
94. Popelka-Filcoff, R.S.; Mauger, A.; Lenehan, C.E.; Walshe, K.; Pring, A. HyLogger™ Near-Infrared Spectral Analysis: A Non-Destructive Mineral Analysis of Aboriginal Australian Objects. *Anal. Methods* **2014**, *6*, 1309–1316. [[CrossRef](#)]
95. Clark, R.N. Spectroscopy of Rocks and Minerals and Principles of Spectroscopy. In *Manual of Remote Sensing*; Wiley: Hoboken, NJ, USA, 1999; ISBN 0471294055.
96. Dooley, K.A.; Lomax, S.; Zeibel, J.G.; Milianni, C.; Ricciardi, P.; Hoenigswald, A.; Loew, M.; Delaney, J.K. Mapping of Egg Yolk and Animal Skin Glue Paint Binders in Early Renaissance Paintings Using near Infrared Reflectance Imaging Spectroscopy. *Analyst* **2013**, *138*, 4838–4848. [[CrossRef](#)]
97. Ghervase, L.; Cortea, I.M. Lighting Up the Heritage Sciences: The Past and Future of Laser-Induced Fluorescence Spectroscopy in the Field of Cultural Goods. *Chemosensors* **2023**, *11*, 100. [[CrossRef](#)]
98. Papiak, Z.E.; Vaccari, L.; Zanini, F.; Sotiropoulou, S. Improving FTIR Imaging Speciation of Organic Compound Residues or Their Degradation Products in Wall Painting Samples, by Introducing a New Thin Section Preparation Strategy Based on Cyclododecane Pre-Treatment. *Anal. Bioanal. Chem.* **2015**, *407*, 5393–5403. [[CrossRef](#)]
99. Gelzo, M.; Corso, G.; Pecce, R.; Arcari, O.; Piccioli, C.; Dello Russo, A.; Arcari, P. An Enhanced Procedure for the Analysis of Organic Binders in Pompeian's Wall Paintings from Insula Occidentalis. *Herit. Sci.* **2019**, *7*, 12. [[CrossRef](#)]
100. Rackham, H. *Pliny Natural History*; Harvard University Press: Cambridge, MA, USA, 1938.
101. Macdonald, B.L.; Hancock, R.G.V.; Cannon, A.; McNeill, F.; Reimer, R.; Pidruczny, A. Elemental Analysis of Ochre Outcrops in Southern British Columbia, Canada. *Archaeometry* **2013**, *55*, 1020–1033. [[CrossRef](#)]
102. Marcaida, I.; Maguregui, M.; Fdez-Ortiz de Vallejuelo, S.; Morillas, H.; Prieto-Taboada, N.; Veneranda, M.; Castro, K.; Madariaga, J.M. In Situ X-Ray Fluorescence-Based Method to Differentiate among Red Ochre Pigments and Yellow Ochre Pigments Thermally Transformed to Red Pigments of Wall Paintings from Pompeii. *Anal. Bioanal. Chem.* **2017**, *409*, 3853–3860. [[CrossRef](#)] [[PubMed](#)]
103. Rakhimol, V.; Maheswari, P.U. Restoration of Ancient Temple Murals using cGAN and PConv Networks. *Comput. Graph.* **2022**, *109*, 100–110. [[CrossRef](#)]
104. Corso, G.; Gelzo, M.; Sanges, C.; Chambery, A.; Di Maro, A.; Severino, V.; Dello Russo, A.; Piccioli, C.; Arcari, P. Polar and Non-Polar Organic Binder Characterization in Pompeian Wall Paintings: Comparison to a Simulated Painting Mimicking an "a Secco" Technique. *Anal. Bioanal. Chem.* **2012**, *402*, 3011–3016. [[CrossRef](#)] [[PubMed](#)]
105. Amadori, M.L.; Barcelli, S.; Poldi, G.; Ferrucci, F.; Andreotti, A.; Baraldi, P.; Colombini, M.P. Invasive and Non-Invasive Analyses for Knowledge and Conservation of Roman Wall Paintings of the Villa of the Papyri in Herculaneum. *Microchem. J.* **2015**, *118*, 183–192. [[CrossRef](#)]

Disclaimer/Publisher's Note: The statements, opinions and data contained in all publications are solely those of the individual author(s) and contributor(s) and not of MDPI and/or the editor(s). MDPI and/or the editor(s) disclaim responsibility for any injury to people or property resulting from any ideas, methods, instructions or products referred to in the content.